

AD A 030770

AFML-TR-76-12

12

FG

STRESS ANALYSIS OF PLASTIC ROTATING BANDS

CALIFORNIA RESEARCH & TECHNOLOGY, INC.
6269 VAHIEL AVENUE, SUITE 200
WOODLAND HILLS, CA 91364

FEBRUARY 1976

TECHNICAL REPORT AFML-TR-76-12
FINAL REPORT FOR PERIOD APRIL 1975 - SEPTEMBER 1975

OCT 15 1976

Approved for public release; distribution unlimited

AIR FORCE MATERIALS LABORATORY
AIR FORCE WRIGHT AERONAUTICAL LABORATORIES
AIR FORCE SYSTEMS COMMAND
WRIGHT-PATTERSON AIR FORCE BASE, OHIO 45433

NOTICE

When Government drawings, specifications, or other data are used for any purpose other than in connection with a definitely related Government procurement operation, the United States Government thereby incurs no responsibility nor any obligation whatsoever; and the fact that the Government may have formulated, furnished, or in any way supplied the said drawings, specifications, or other data, is not to be regarded by implication or otherwise as in any manner licensing the holder or any other person or corporation, or conveying any rights or permission to manufacture, use, or sell any patented invention that may be related in any way thereto.

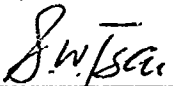
This report has been reviewed by the Information Office (OI) and is releasable to the National Technical Information Service (NTIS). At NTIS, it will be available to the general public, including foreign nations.

This technical report has been reviewed and is approved for publication.



S. W. Tsai
Project Monitor

FOR THE DIRECTOR



S. W. Tsai, Chief
Mechanics & Surface Interactions Branch
Nonmetallic Materials Division

Copies of this report should not be returned unless return is required by security considerations, contractual obligations, or notice on a specific document.

UNCLASSIFIED

SECURITY CLASSIFICATION OF THIS PAGE (When Data Entered)

19 REPORT DOCUMENTATION PAGE		READ INSTRUCTIONS BEFORE COMPLETING FORM	
18 2 APML (CR-76-12)	3 GOVT ACCESSION NO.	4 AUTHORITY	5 PRIME CONTRACT NUMBER
6 7 STRESS ANALYSIS OF PLASTIC ROTATING BANDS	8 PERFORMING ORGANIZATION NAME AND ADDRESS California Research & Technology, Inc. 6269 Varial Avenue, Suite 200 Woodland Hills, CA 91364	9 TYPE OF REPORT & PERIOD COVERED Final Report, 1 Apr 1975 - 30 Sep 1975	10 PROGRAM ELEMENT PROJECT TASK AREA & WORK UNIT NUMBERS ILIR0073
10 11 M. H. Wagner K. N. Kroeyenhagen	12 CONTROLLING OFFICE NAME AND ADDRESS Air Force Materials Laboratory (AFML/MEH) Air Force Wright Aeronautical Laboratories Wright-Patterson AFB, Ohio 45433	13 GRANT NUMBER(S) F33615-75-C-5286 NEW	14 AUTHORITY
12 13 Same	14 15 12 95p.	16 MONITORING AGENCY NAME & ADDRESS (if different from Controlling Office) Same	17 SECURITY CLASS (of this report) Unclassified
18 DISTRIBUTION STATEMENT (of this Report) Approved for public release; distribution unlimited.			
16 19 ILIR-00-73			
20 DISTRIBUTION STATEMENT (of the abstract) in Block 29, if different from Report) Same			
21 SUPPLEMENTARY NOTES			
22 KEY WORDS (Continue on reverse side if necessary and identify by block number) interior ballistics rotating bands dynamic stress analysis finite-difference codes			
23 ABSTRACT (Continue on reverse side if necessary and identify by block number) Dynamic stress analyses of plastic rotating bands, used on projectiles to impart spin, have been obtained by means of a two-dimensional finite-difference computer code. The first phase of the interaction within the barrel, involving the axisymmetric convergence of the plastic band into the forcing cone, has been investigated in this study. Numerical solutions for three rotating band problems were obtained. The results of these solutions showed that (a) shearing forces acting along the band/barrel interface due to			

FORM 1 JAN 73 1473 EDITION OF 1 NOV 65 IS OBSOLETE

UNCLASSIFIED
SECURITY CLASSIFICATION OF THIS PAGE (When Data Entered)

391223

over
13

UNCLASSIFIED

SECURITY CLASSIFICATION OF THIS PAGE(When Data Entered)

friction can have a major effect on rotating band performance, and (b) that with a current band design, the sharply-beveled rear section of the band becomes grossly distorted and develops a large angular lip protruding from the rear of the band (i.e., feathering). The third case considered a design modification made to alleviate the extrusion problem. These initial analyses show that finite-difference code solutions of the dynamics of rotating bands are practical and can provide a useful tool to investigate a number of key factors bearing on plastic band performance, such as material properties, stress-strain conditions experienced, and band geometries.



UNCLASSIFIED

SECURITY CLASSIFICATION OF THIS PAGE(When Data Entered)

PREFACE

This report describes a research program to analyze the dynamic stresses and deformations in plastic rotating bands (such as used on projectiles) as they are forced into a converging forcing cone at high speed. A two-dimensional finite-difference computer code was used for the analyses. The program was conducted during the period April through September 1975, at California Research & Technology, Inc. 6269 Variel Ave., Woodland Hills, CA 91364, under Contract F33615-75-C-5206, initiated under Task No. ILIR0073. The research was performed by M. H. Wagner and K. N. Kreyenhagen. W. S. Goerke, C. K. Wilson, and C.C. Fulton provided assistance in code development and programming. The Project Engineer for the Air Force Materials Laboratory was S. W. Tsai, Chief, Mechanics & Surface Interactions Branch, Nonmetallic Materials Division (AFML/MBM). The authors submitted this report in October 1975.

TABLE OF CONTENTS

	<u>Page</u>
SECTION I. INTRODUCTION, SUMMARY AND RECOMMENDATIONS	1
A BACKGROUND	1
B OBJECTIVES.	3
C NUMERICAL APPROACH FOR DYNAMIC STRESS ANALYSIS.	3
D SUMMARY OF RESULTS.	5
E CONCLUSIONS AND RECOMMENDATIONS	7
1 Utility of Numerical Analysis of Dynamic Stresses and Distortions in Rotating Bands	7
2 Recommendations.	9
SECTION II. NUMERICAL SOLUTIONS	12
A PROBLEM DEFINITION.	12
B MATERIAL PROPERTIES	13
C NUMERICAL METHOD.	14
D NUMERICAL SOLUTION OF CASE 1 - PLASTIC BAND INTERACTION WITH FRICTION	15
E NUMERICAL SOLUTION OF CASE 2 - PLASTIC BAND INTERACTION WITHOUT FRICTION.	16
F NUMERICAL SOLUTION OF CASE 3 - MODIFIED PLASTIC BAND DESIGN	18
APPENDIX A: PRINCIPAL STRESS FIELD PLOTS	57
APPENDIX B: TIME HISTORIES OF STRESS AND VELOCITY.	66
REFERENCES	86

LIST OF ILLUSTRATIONS

<u>Figure</u>	<u>Page</u>
1. Field of Analysis for Computations of a Projectile/Rotating Band Tunneling into a Forcing Cone	21
2. Problem Conditions for Numerical Solutions	22
3. Deformation and Flow in Plastic Band at 11.4 μ sec, Case 2 (Baseline design, no friction).	23
4. Deformation and Flow in Plastic Band at 7.7 μ sec, Case 3 (Modified design)	24
5. Deformation of Plastic Band at 20.7 and 27.6 μ sec, Case 3 (Modified design)	25
6. Axial Force at Band/Barrel Interface vs Time for Baseline and Modified Plastic Band Designs	26
7. Suggested Method for Plane Strain Analysis of Rotating Band-Rifling Interaction.	27
8. Baseline Plastic Band Geometry and Computational Grid (Cases 1 and 2 - Baseline Design)	28
9. Grid Configuration at 1.5 μ sec, Case with Friction (Case 1 - Baseline Design).	29
10. Velocity Field at 1.5 μ sec, Case with Friction (Case 1 - Baseline Design)	30
11. Grid Configuration at 3.6 μ sec, Case with Friction (Case 1 - Baseline Design)	31
12. Velocity Field at 3.6 μ sec, Case with Friction (Case 1 - Baseline Design)	32
13. Velocity Field at 1.5 μ sec, Case without Friction (Case 2 - Baseline Design)	33
14. Grid Configuration at 3.1 μ sec, Case without Friction (Case 2 - Baseline Design).	34

LIST OF ILLUSTRATIONS (Cont'd.)

<u>Figure</u>	<u>Page</u>
15. Velocity Field at 3.1 μ sec, Case without Friction (Case 2 - Baseline Design)	35
16. Grid Configuration at 7.9 μ sec, Case without Friction (Case 2 - Baseline Design).	36
17. Velocity Field at 7.9 μ sec, Case without Friction (Case 2 - Baseline Design)	37
18. Grid Configuration at 11.4 μ sec, Case without Friction (Case 2 - Baseline Design).	38
19. Velocity Field at 11.4 μ sec, Case without Friction (Case 2 - Baseline Design).	39
20. Grid Configuration at Rear Section of Plastic Band at 11.4 μ sec, Case without Friction (Case 2 - Baseline Design)	40
21. Comparison of Axial Forces on Barrel with and without Surface Friction (Cases 1 and 2 - Baseline Design)	41
22. Comparison of Radial Forces on Barrel with and without Surface Friction (Cases 1 and 2 - Baseline Design)	42
23. Axial Force at Band/Barrel Interface vs Time, Case without Friction (Case 2 - Baseline Design) .	43
24. Radial Force at Band/Barrel Interface vs Time, Case without Friction (Case 2 - Baseline Design) .	44
25. Normal Stress (σ_n) and Tangential Stress (τ) Distributions on Barrel, Case with Friction (Case 1 - Baseline Design)	45
26. Normal Stress (σ_n) Distributions on Barrel, Case without Friction (Case 2 - Baseline Design) .	46
27. Modified Plastic Band Geometry and Computational Grid (Case 3 - Modified Design).	47

LIST OF ILLUSTRATIONS (Cont'd.)

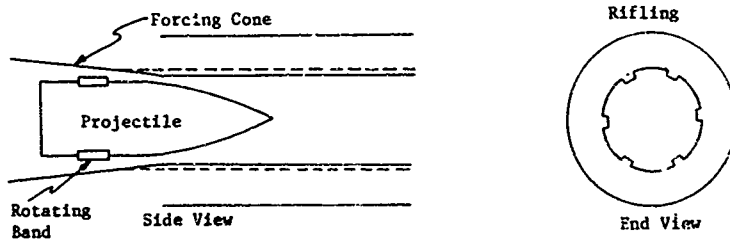
<u>Figure</u>	<u>Page</u>
28. Grid Configuration at 7.7 μ sec, Modified Plastic Band Design (Case 3)	48
29. Velocity Field at 7.7 μ sec, Modified Plastic Band Design (Case 3)	49
30. Grid Configuration at 15.5 μ sec, Modified Plastic Band Design (Case 3)	50
31. Grid Configuration at 20.7 μ sec, Modified Plastic Band Design (Case 3)	51
32. Grid Configuration at 27.6 μ sec, Modified Plastic Band Design (Case 3)	52
33. Velocity Field at 27.6 μ sec, Modified Plastic Band Design (Case 3)	53
34. Radial Force at Band/Barrel Interface vs Time for Baseline and Modified Plastic Band Designs . . .	54
35. Distributions of Normal Stress along Band/Barrel Interface, Modified Plastic Band Design.	55
36. Peak Compressive Stresses within Band, Baseline and Modified Plastic Band Designs (Cases 2 and 3). .	56

SECTION I

INTRODUCTION, SUMMARY, AND RECOMMENDATIONS

A. BACKGROUND

Rotating bands are used on projectiles to impart spin (by transmitting torque from rifling to the projectile), to improve the propellant gas seal, and to reduce wear of the barrel (by minimizing direct contact between the hard projectile and the walls). Rotating bands must generally be of pliable and/or ductile material, since they must withstand substantial plastic flow in accommodating to the barrel and to the rifling. The material must also have sufficient strength to resist the propellant gas pressure, to transmit torque to the projectile, and to remain attached to the rotating projectile as it leaves the muzzle.



This sketch (not to scale) shows a typical rotating band. The projectile is somewhat smaller than the minor diameter of the bore, but the OD of the rotating band is larger, so that there is dimensional interference. When the projectile is fired, it "tunnels" into a forcing cone where the rotating band is squeezed down until it fits into the barrel. To accomplish this squeezing, the rotating band material:

- (1) *flows circumferentially* into the rifling grooves
- (2) *is compressed* radially under the high confining pressure of the barrel
- (3) *Flows axially* to relieve the volumetric compression (i.e., the rotating band becomes longer).

Within the barrel, the rifling can have either a fixed or a variable twist (pitch) along the barrel length. This twist, acting through the rotating band, imparts angular acceleration as the projectile itself undergoes linear acceleration down the barrel. As the projectile leaves the muzzle, the radial compression of the band is relaxed. The band remains attached to the projectile until it reaches the target.

Some nylon-type plastics are desirable materials for rotating bands, and they are successfully used in this application. However, failures of nylon rotating bands have been experienced, especially in projectiles which are designed to reach higher muzzle velocities. Information about the timing of such failures (i.e., the location within the barrel at which failure occurs) and the cause thereof is not available, nor is it readily attainable through experiments. Such information is needed in order to design better rotating band-rifling systems, and in order to select or develop better materials for rotating bands.

Numerical hydro-elastic-plastic code analyses of the dynamics of rotating band distortion as the projectile funnels into the forcing cone provide an approach for obtaining information about the dynamic stresses and deformations in rotating bands. This report presents the results of three such analyses.

P. OBJECTIVES

The objectives of this preliminary program were:

- (1) To adapt a two-dimensional numerical code for analysis of the axisymmetric stresses and distortions of rotating bands entering the forcing cone,
- (2) Through analyses of a representative, or "baseline" rotating band design, to show the utility of numerical dynamic stress and deformation analyses as a tool for designing, evaluating, and improving rotating bands, and
- (3) To identify the stress and deformation histories experienced in critical regions in the representative rotating band design.

C. NUMERICAL APPROACH FOR DYNAMIC STRESS ANALYSIS

When the projectile enters the barrel, the significant interference fit requires that the rotating band be severely compressed and that it be deformed in a very short interval of time. To accommodate the nonlinear, dynamic processes involved, a finite-difference code was used, specifically, the CRT WAVE-L code. This is a Lagrangian code based on Wilkins' HEMP method.¹ The WAVE-L code has been applied to a wide range of impulsive loading problems, including hypersonic impact,^{2,3} projectile penetration,^{4,5} and dynamic stress analysis.⁶

WAVE-L is a "first principle" code which obtains "time-marching" solutions of the conservation equations and the

constitutive equations describing the properties (elastic, plastic, and fracture) of the materials involved. The code is two-dimensional, i.e., problems must be described in two space dimensions. This includes 2-D plane strain problems, as well as 3-D problems which are axisymmetric.

The geometry of the projectile/rotating band tunneling into a smooth-walled forcing cone and traveling through a smooth bore is axisymmetric, and can thus be described using two space dimensions. When rifling grooves in the barrel are encountered, however, the problem is no longer strictly axisymmetric, in that 3-D non-symmetrical effects occur (i.e., circumferential flow). In the present study, we have decoupled the problem, treating only the axisymmetric aspects of the initial tunneling processes.

(A separate but coupled plane strain analysis can be made of the non-symmetric interactions between the rotating band and the rifling in the barrel. Recommendations for this type analysis, together with a suggested approach, are given in Section I E1 of this report.)

Figure 1 is a schematic defining the computational field for analysis of a projectile/rotating band tunneling into a forcing cone. It is assumed that neither the projectile nor the barrel deform significantly, so they are treated as rigid boundaries which confine and deform the nylon rotating band. (This is a reasonable assumption; the distortions in the barrel and projectile due to stress levels imposed as the nylon compresses are very small compared to the rotating band distortions.) The actual field of analysis can thus be confined to the rotating band itself.

For the code analysis, the geometry of the rotating band slot (i.e., the slot in the projectile containing the

rotating band) and the geometry of the forcing cone are specified, as well as the velocity at which the projectile is moving. For the present analysis, this was specified to be 500 fps. (For convenience in possible future comparisons with experiments, the projectile was assumed to be stationary, with the barrel moving over it at 500 fps. This transformation has no effect on the stresses in the rotating band.)

The rotating band itself is described by a Lagrangian network of computational cells, and by a set of equations (based on measured properties) which characterize the elastic and plastic stress-strain behavior of the rotating band material (in the cases treated here, Nylon 6/12.) No failure criteria were used in these analyses, although the capability to treat certain types of failure exists in the WAVE-L code.

D. SUMMARY OF RESULTS

Numerical solutions were performed for three rotating band problems as defined in Figure 2. The baseline design (Cases 1 and 2) approximately corresponds with the rotating band for a 20mm M-56 projectile. Representative major and minor diameters for a 20mm barrel are .817 in. and .786 in., respectively. The nominal barrel diameter ($D_b = .809$ in.) chosen for these axisymmetric analyses gives the same overall volumetric compression of the rotating band entering the forcing cone as occurs in a rifled barrel.

The presence of friction (coefficient $\mu = 0.1$) in Case 1 produced almost immediate locking between the nylon and the forcing cone. This was because the normal stresses, σ_n , across the converging interface build up very quickly to the level where $\mu\sigma_n$ exceeds the shear strength of the nylon. Nylon near the interface thereafter distorts at

essentially the full projectile-barrel relative velocity. This clearly shows that friction can be very important in rotating band design. However, we consider the results of Case 1 to be an exaggerated indication of the effects of friction, at least in a plastic material like nylon. Initial friction and plastic distortion will produce significant heating of the surface, thereby softening or melting the material such that the surface cannot thereafter support large frictional stresses.

We did not have properties to quantitatively define this softening and weakening of the surface; it appeared reasonable for the purposes of these analyses to assume that the friction becomes so small as to be negligible. In Case 2, we therefore repeated the analysis of the baseline rotating band design, with no friction. Figure 3 indicates the way in which the frictionless basic band distorts as it tunnels into the forcing cone. The nylon is initially squeezed inward. The stress on the surface of the nylon builds up to about 40,000 psi. This compression causes the nylon to begin to flow rearward, producing gross distortion of the sharply-beveled trailing surface, as seen in Figure 3. As a result, nylon extrudes out of the rotating band slot and into the converging region between the projectile and forcing cone walls. Eventually, this will lead to a very thin, probably irregular annulus of nylon between the aft end of the projectile and the barrel (i.e., feathering). Portions of this badly extruded annulus may break off, either in the barrel or after the projectile leaves the muzzle. Presumably this irregular extrusion will have undesirable effects on the in-flight aerodynamics of the projectile.

To avoid, or at least lessen, the rearward extrusion of nylon out of the rotating band slot, a modified design was considered (Case 3). As seen in Figure 2, this design substituted a more gradual slope for the trailing surface. Figures 4 and 5 show the pattern of distortion which develops in the modified design. The gradually-sloping trailing surface bulges out towards the forcing cone. Some rearward extrusion of nylon out of the rotating band slot eventually occurs, but it is greatly reduced, as compared to the basic design.

Figure 6 compares the axial force history applied to the projectile by the basic and the modified rotating band designs. The force is higher in the modified case because the more gradual trailing surface closes against the forcing cone, thereby increasing the surface area of the rotating band which acts on the forcing cone. The increased force does not appreciably affect the projectile dynamics, however; the impulse transmitted to the projectile with the modified rotating band as it tunnels into the forcing cone will affect its velocity by only about 1 fps.

Detailed information about the stresses and distortions in the basic design (Case 2) and the modified design (Case 3) is given in the text and in the appendices. This includes time histories of the stresses at several points within the rotating bands.

E. CONCLUSIONS AND RECOMMENDATIONS

1. Utility of Numerical Analysis of Dynamic Stresses and Distortions in Rotating Bands

The three analyses which were performed show that finite-difference solutions of rotating bands tunneling

into forcing cones are practical, and are specifically useful for these purposes:

- o To identify material properties which have major effects on design and performance
- o To identify stress-strain conditions which are experienced by rotating band materials
- o To identify design weaknesses
- o To suggest methods for correcting such weaknesses
- o To evaluate design modifications.

Examples of these uses are seen in the three cases which were analyzed:

In Case 1, a code solution was used to *identify a critical material property* (friction), showing that it can have a major effect on rotating band design and performance. (The lack of data on frictional properties for candidate materials under pertinent conditions of stress, temperature, and sliding velocity is a deficiency which needs to be remedied. The pertinent conditions for these and other property measurements can be determined from numerical solutions.)

In Case 2, a code solution was used to *identify a design weakness* in the baseline rotating band geometry, and to *suggest a means for correcting the problem*. (The sharply-beveled trailing surface of the baseline geometry leads to gross distortion and eventually to extrusion of material out of the rotating band slot and into the narrowing region between the projectile and the barrel. A more gradual slope for the trailing surface may alleviate this problem.)

In Case 3, a code solution was used to *evaluate a possible design improvement* in the baseline geometry. (This improvement involved the gradually sloping trailing surface. It greatly reduced, but did not wholly eliminate, the extrusion problem.)

In all the cases, *stress and strain levels, and strain rates were determined at several stations.* (Maximum compressive stresses were of the order of 2.5 kb, or about 38,000 psi. Maximum strain rates in these 500-fps cases were of the order of $10^4 - 10^5$ /sec.)

2. Recommendations

Applications. The above uses of the code can be of substantial value in design and evaluation, and in material selection or development. These applications should be pursued.

- o Candidate new designs, as well as existing designs which are not performing well, should be analyzed to identify critical regions where failures may occur. Possible design modifications should then be numerically evaluated.
- o A systematic study should be made to determine the desirable mechanical property attributes of rotating band materials.

Code Validation. Although the basic WAVE-L numerical method has been validated in a number of prior experimental comparisons for other applications, it would be desirable to verify the ability of the code (and material models) to predict

rotating band processes. A possible experiment would involve reverse ballistic firing of a "barrel" over a fixed "projectile" which is supported on a rod.* Force-time measurements could be made in the support rod as the barrel pushes over the projectile.

Interactions with Rifling. In addition to the axisymmetric processes occurring as the rotating band is squeezed into the barrel (which are analyzed in the three cases treated so far), non-symmetric processes are involved as the rifling lands force deep grooves into the rotating band, and as the projectile travels down the barrel. These processes involve circumferential flow of material as the rifling lands impinge into the band, and the application of tangential forces to the rotating band by the twist of the rifling.

Analyses of the stresses and deformations in rotating bands due to these asymmetric processes should be made. A possible approach would be to treat the problem in plane strain, as indicated in Figure 7. In this approach, the projectile would be represented by the rigid-body central core, and the barrel would also be represented as a rigid body (concentric to the core). The rotating band (between the rigid projectile and barrel) would be described with the elastic-plastic rotating band material properties.

* This experiment has been suggested by H. Swift of UDR!

There would be a sliding interface between the band and the barrel. Friction could be specified in the z -direction (*perpendicular* to the plane of solution), thereby allowing the effects of sliding friction in the third dimension (z -direction) to be incorporated in the plane strain solution. The band would be locked to the projectile body.

Initially, the rifling lands, as represented by the periodic protrusions around the rigid barrel, would be nonexistent (i.e., the barrel surface would be smooth). The flat surfaces would thereafter be gradually forced into the rotating band by prescribing their displacement, $r(t)$ a function of time. The angular acceleration produced by the rifling would be represented by prescribing rotating of the barrel by $\omega(t)$, as determined by the projectile velocity and by the pitch of the rifling.

The same types of information could be obtained from the plane strain solutions as from the axisymmetric solutions which are described in the report; i.e., field plots of distortions, particle velocities, and principal stresses, and parameter vs time plots at selected stations.

SECTION II

NUMERICAL SOLUTIONS

A. PROBLEM DEFINITION

A representative "baseline" rotating band of interest was chosen as an initial vehicle to test and demonstrate the finite-difference code technique of analysis. This is illustrated in Figure 1 (page 21). The specific baseline dimensions, and the computational grid used to represent the band, are shown in Figure 8. The band design shown is one which has been considered for a 20mm M-56 projectile.

The analyses which were performed were confined to the axisymmetric convergence of the band as it engaged with the forcing cone, and therefore did not explicitly treat the rifling. Instead, a uniform barrel diameter (.809 in.), between the major and minor diameters of the barrel (.817 in. and .786 in., respectively), was chosen which provides the same overall volumetric compression of the rotating band as occurs in the rifled barrel. The initial .829-in. OD of the rotating band is thus subjected to a maximum radial convergence of .010 in. in the forcing cone.

A nominal constant 500 fps was chosen for the velocity at which the projectile enters the forcing cone. In the actual gun firing, the projectile is accelerated from an initial rest position during the tunneling process. This mode of engagement can be handled by the code, but we did not have information defining a typical acceleration-time history in the forcing cone. This problem is not felt to be particularly

sensitive to velocity, so long as the velocity is anywhere in the low subsonic range (which covers the range of velocities of interest here), and so long as the material properties are not rate sensitive (as was the case with the material model used in these analyses).

In the code solution, the forcing cone and barrel were set up to move at the prescribed velocity, and the projectile was fixed. This was done for convenience and efficiency, since it immediately gives the flow in the band due to the interaction, rather than centering the flow about the projectile velocity. This arrangement also corresponds to a reverse ballistic laboratory test (in which the band is mounted on rigid rod, and a heavy ring simulating the barrel is projected against the band), which could be used to confirm the validity of the code solutions.

B. MATERIAL PROPERTIES

A material of current interest, Nylon 6/12, was chosen for the plastic band. The following initial value properties were employed in the code solution for this material:⁷

$$\text{Density, } \rho_0 = 1.08 \text{ gm/cm}^3$$

$$\text{Young's modulus, } E = 300 \text{ ksi} = 20.7 \text{ kb}$$

$$\text{Poisson's ratio, } \nu = .4$$

These values imply the following other properties:

$$\text{Bulk modulus, } K = 500 \text{ ksi} = 34.5 \text{ kb}$$

$$\text{Shear modulus, } G = 107 \text{ ksi} = 7.4 \text{ kb}$$

$$\begin{aligned} \text{Dilatational wave speed, } c_p &= 6646 \text{ ft/sec} \\ &= 2026 \text{ m/sec.} \end{aligned}$$

The equation of state was assumed to be linear elastic. An elastic-plastic constitutive model was used, employing the von Mises yield criterion and a non-associated flow rule. The value of yield strength used was 16.4 ksi (1.13 kb). Tensile stress was limited by imposing a minimum value for hydrostatic tension, $P_{\min} = -2.93$ ksi (-.202 kb). Under uniaxial stress, this gives a maximum permissible tensile stress of 8.8 ksi (.61 kb), corresponding to the tensile strength of the material.

The steel projectile and barrel were treated as rigid bodies. The plastic band was assumed to be locked to the projectile all along the mating interface.

In the Case 1 analysis, shearing forces due to friction were generated at the band/barrel interface, in addition to the normal forces developed as the band is deformed. A nominal constant value for the coefficient of friction of 0.1 was used. Cases 2 and 3 were run with no friction, both for comparison and to provide a lower bound on the shear deformation of the band surface. (The solution results from Case 1 indicated that the frictional effects resulting from a friction coefficient of 0.1 were excessive.)

C. NUMERICAL METHOD

The WAVE-L code was employed for these calculations. WAVE-L is a two-dimensional code which solves the equations of motion for elastic-plastic bodies by means of a finite-difference Lagrangian-cell technique. The mathematical formulation is basically the same as that described by Wilkins.¹ An important feature of the code is its provision for sliding interfaces. (In a normal Lagrangian grid, the cells are locked together, and no sliding can occur.)

A sliding interface was used for the band/barrel interface. Another important capability of WAVE-L is its ability to treat moving rigid bodies (in this case, the barrel). The code computes the loading forces on the rigid body and thus the deceleration can be included in the calculations, given the mass of the rigid body. This rigid-body formulation was previously developed to treat the penetration dynamics of projectiles.^{4,5} Some additional development of the code was required to handle the plastic band interaction geometry.

D. NUMERICAL SOLUTION OF CASE 1 - PLASTIC BAND INTERACTION WITH FRICTION

The initial Lagrangian grid configuration set up for the problem described above is shown in Figure 8. The plastic band was resolved with 8 cells across its width and 53 cells along its length. One hundred six lattice points were used along the barrel to compute the distribution of stresses and force components acting on the barrel.

The code results of this first case, which included frictional effects, are depicted in Figures 9 to 12, which are plots of the grid configuration and velocity field in the band for times of 1.5 and 3.6 usec.

The plots of the grid also show which material is currently undergoing plastic deformation; i.e., is on the yield surface. This is denoted by cells containing an x or $+$, with x indicating a compressive pressure, $P > 0$, and $+$ indicating hydrostatic tension, $P < 0$.

The velocity vector field plots show the direction and magnitude of the particle velocity at each lattice point in the computing grid.

These results show that a strong upward axial flow is induced in the band next to the contact surface. Note that the band surface appears to be dragged along by the barrel, causing severe distortion of the material next to the band. The frictional forces built up across the interface were sufficient to lock a portion of the nylon surface onto the barrel, so that the surface was actually moving upward at the full barrel velocity. This clearly shows that friction is important, and indicates that frictional properties under high stress, high velocity conditions need to be defined. However, we consider the results obtained in Case 1 to be an exaggeration of the actual frictional effects. Since there is a significant heating of the surface due to friction and plastic deformation, it is likely that the surface material softens such that it could not support frictional stresses as large as that computed with a coefficient of friction of 0.1. It was thus decided to discontinue the running of Case 1 and to instead run a second case, with no friction.

Additional results of Case 1 are given in the next section in comparative plots.

E. NUMERICAL SOLUTION OF CASE 2 - PLASTIC BAND INTERACTION WITHOUT FRICTION

The problem conditions for Case 2 were kept exactly the same as for Case 1, except that the band/barrel interface was assumed to be frictionless. Thus no shearing forces are generated at the interface.

The results of the code solution for this case are depicted in Figures 13 to 19, which show plots of the grid configuration and/or velocity field for times of 1.5, 3.1, 7.9, and 11.4 μ sec. Note that the early time flow is now radially inward, as opposed to the strong axial flow seen in the case with friction. At later times, however, a strong axial flow occurs, as the upper end of the band is extruded into the open cone.

By 7.9 μ sec, the extrusion action at the rear of the band had produced such severe grid distortion that the solution could not be continued. To allow continued integration, a rezone of the grid was performed. Rezones are used to reposition the computational grid in a distorted region so as to give more regular cell shapes; a comprehensive rezone processor correctly redistributes the cell variables among the new cells. Code modifications required to treat rezones of the plastic band problem were developed and checked out for this first rezone and will be available in the future as needed.

Following the rezone, the solution was continued out to a time of 11.4 μ sec. The extrusion action noted earlier in the solution continued in this later phase of the solution, causing formation of a pronounced annular lip protruding out from the rear of the band. The presence of such a lip would presumably degrade the aerodynamic stability of the bullet. The solution was terminated at this point, since the behavioral pattern of this band design was clear (for this material) and because the axial forces were significantly diminished. An enlarged view of the extruded rear section of the band at the end of the solution is shown in Figure 20. As the projectile moves

further into the converging forcing cone, this extruded annulus would become thinner and longer.

Comparative time histories of the axial and radial forces acting at the band/barrel interface for Cases 1 and 2 (with and without friction), are shown in Figures 21 and 22. Figure 21 shows the increase in axial force at early times caused by friction. However, by 5.5 μ sec, the axial force in the case without friction surpasses that with friction. Significantly higher normal stresses build up in the case without friction, since the band material next to the barrel does not flow up (axially) as much, and is thus subjected to greater radial compression by the forcing cone. Complete time histories of the axial and radial forces for Case 2 are shown in Figures 23 and 24. The peak axial force was 840 lb, occurring at 5.6 μ sec, and the peak radial force was 1670 lb/rad, occurring at 6.7 μ sec. At 11.4 μ sec, at the end of the solution, the axial force had dropped off to 15% of its peak value.

Stress distributions on the forcing cone are shown in Figures 25 and 26 for the two cases.

F. NUMERICAL SOLUTION OF CASE 3 - MODIFIED PLASTIC BAND DESIGN

The solution results of Case 2 indicated that the band distortion was concentrated at the junction of the 45° beveled rear section and the projectile. For the purpose of alleviating the severe distortion occurring at the rear of the band, it was decided to evaluate the behavior of a modified design, having a longer, more gradual sloping rear section. The modified design is shown in Figure 27. It has a long, 10° sloping rear section replacing the 45°

beveled section of the original design. The flat section and the 6° sloping forward section making initial contact with the forcing cone were kept the same as in the baseline design so as to isolate the effect of the modified rear section. The front of the band ahead of the start of the forcing cone was shortened, since it has little effect on the problem dynamics. The overall length of the modified band was .32 in., compared with .28 in. for the baseline design.

The initial Lagrangian grid for the code solution of Case 3 is also indicated in Figure 27. The zoning was kept the same as in the previous problem; i.e., 8 cells across the width of the band. Fifty-nine cells were used along its length.

The results of the Case 3 solution were very interesting: with the long, shallow-sloping rear section, the response of the band was much more regular, smoothly bowing out as it was forced back. The solution was carried out to 27.6 μ sec, by which time the axial relative displacement of the band/barrel was .166 in. As an indication of the uniform deformation behavior, no rezones of the grid were required during this period. (In the previous problem, severe distortion necessitated a rezone at 7.9 μ sec.) A sequence of the band/barrel configurations and/or velocity fields for times of 7.7, 15.5, 20.7, and 27.6 μ sec are shown in Figures 28 to 33. By 27.6 μ sec, some distortion has built up, at the rear of the band, but it is less than seen with the previous design.

Time histories of the axial and radial forces at the band/barrel interface in the modified design (Case 3) are

shown in figures 6 and 34, plus those for the baseline design (case 2) for comparison. At early times, the response is seen to be the same, confirming that the geometry of the initial contact surface was the same between the two problems. The modified design produces a significantly longer force pulse, corresponding to the increased length of band behind the forcing tip (.27 in. compared with .17 in.). Also, the band bows out until it reaches the forcing cone. The resulting high pressure between the band and the cone produces a large axial force. Assuming a projectile weight of .4 lb, the peak deceleration imparted to the projectile due to convergence in the modified design is ~2000 g's. This deceleration for 20 μ sec would reduce the projectile velocity by 1.3 fps.

Distributions of the normal stress along the band/cylinder interface for several times are shown in Figure 35.

The peak stress levels experienced within the band during the interaction are indicated in Figure 36. The peak compressive stresses along the inner and outer edge of the band about midway across the band vs axial distance are plotted. Also shown for comparison are the corresponding stresses for the baseline band design.

Additional results from the numerical solutions are given in the Appendices.

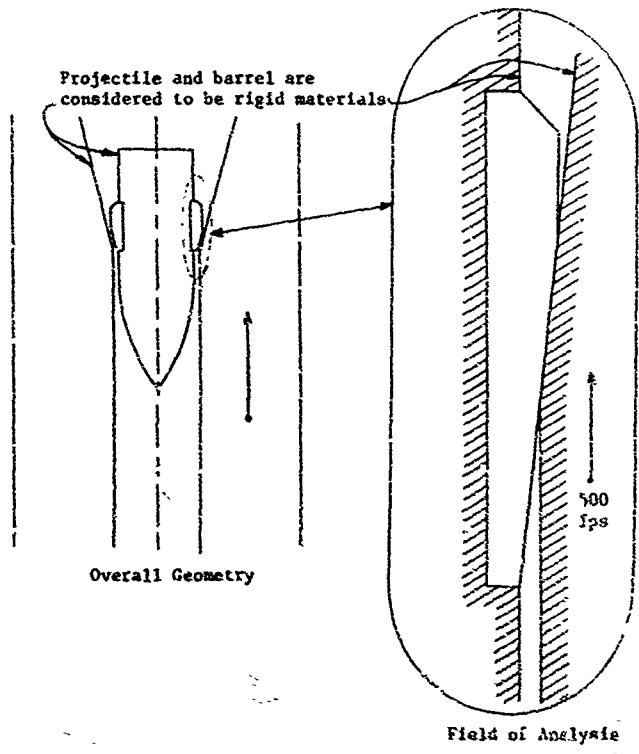


Figure 1. Field of Analysis for Computations of a Projectile/Rotating Band Tunneling into a Forcing Cone

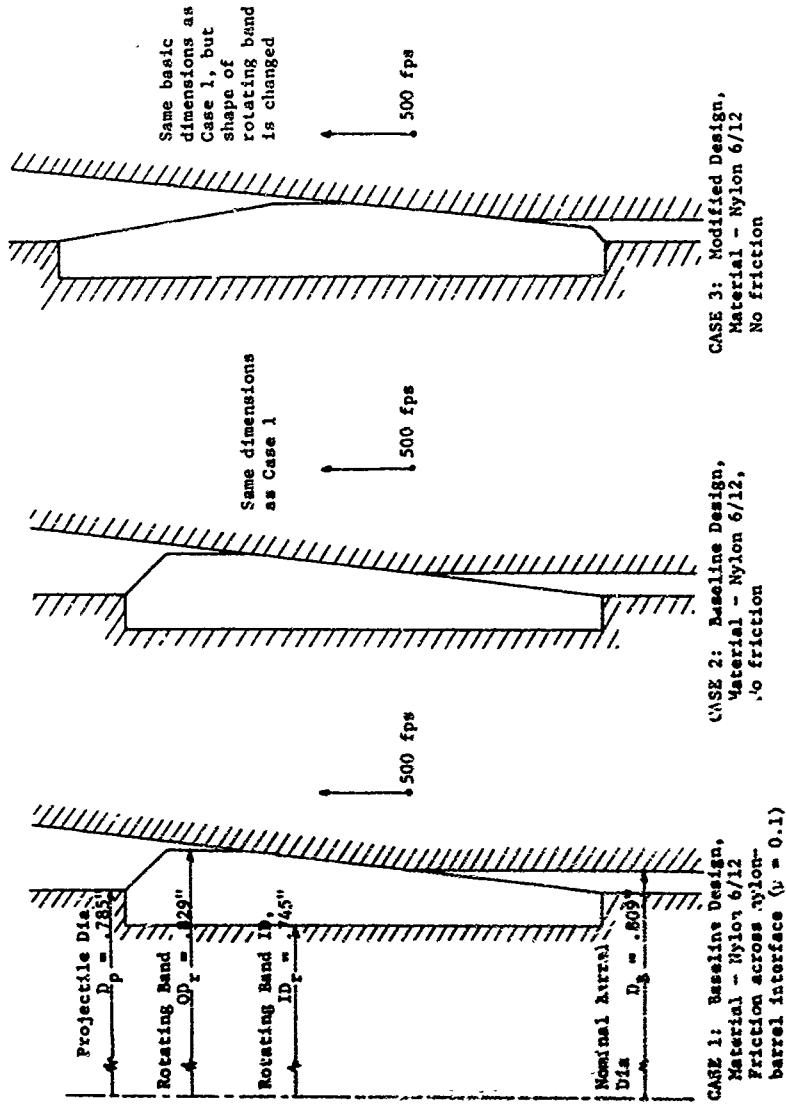


Figure 2. Problem Conditions for Numerical Solutions

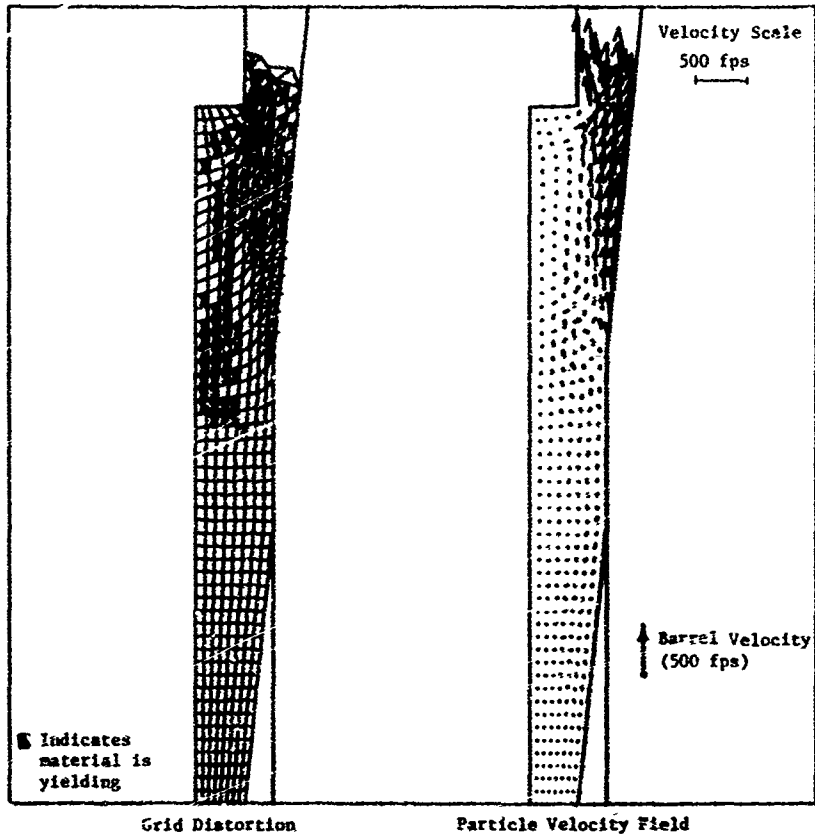


Figure 3. Deformation and Flow in Plastic Bend at 11.4 usec, Case 2
(Baseline design, no friction)

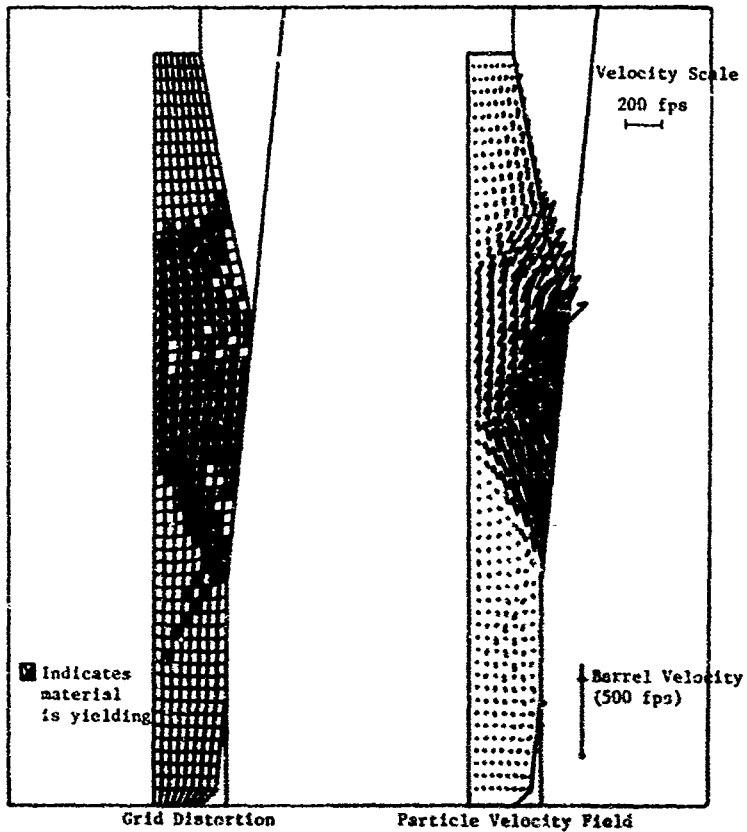


Figure 4. Deformation and Flow in Plastic Band at 7.7 usec, Case 3 (Modified design)

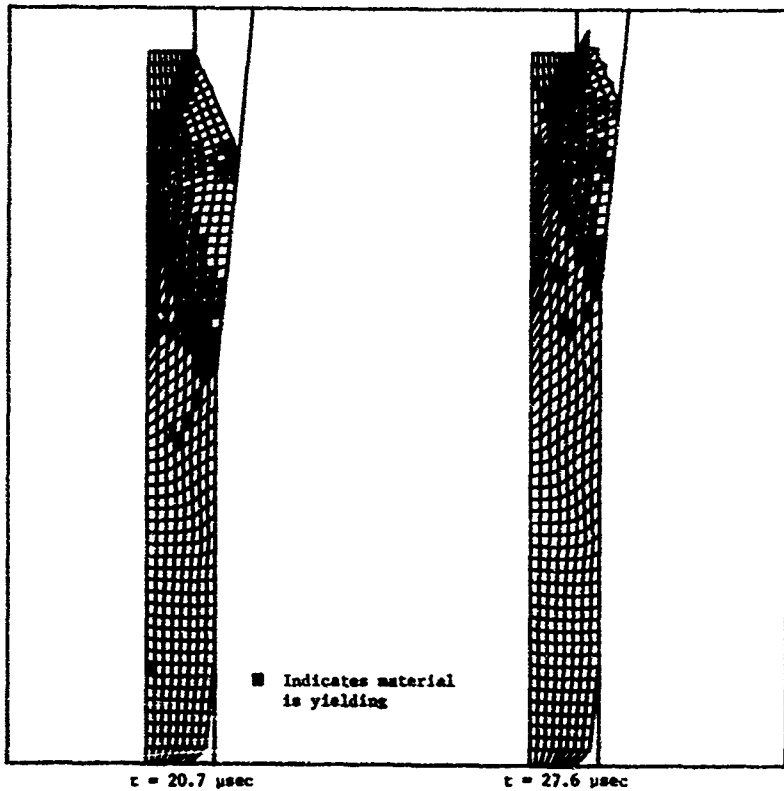


Figure 5. Deformation of Plastic Band at 20.7 and 27.6 μsec , Case 3 (Modified Design)

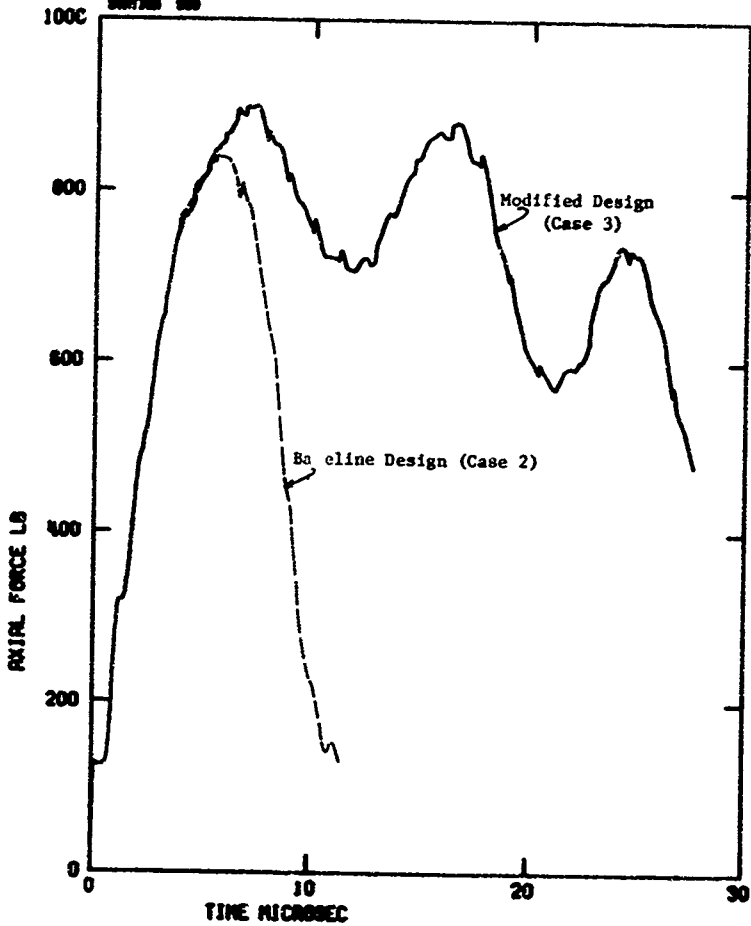


Figure 6 . Axial Force at Band/Barrel Interface vs Time for Baseline and Modified Plastic Band Designs

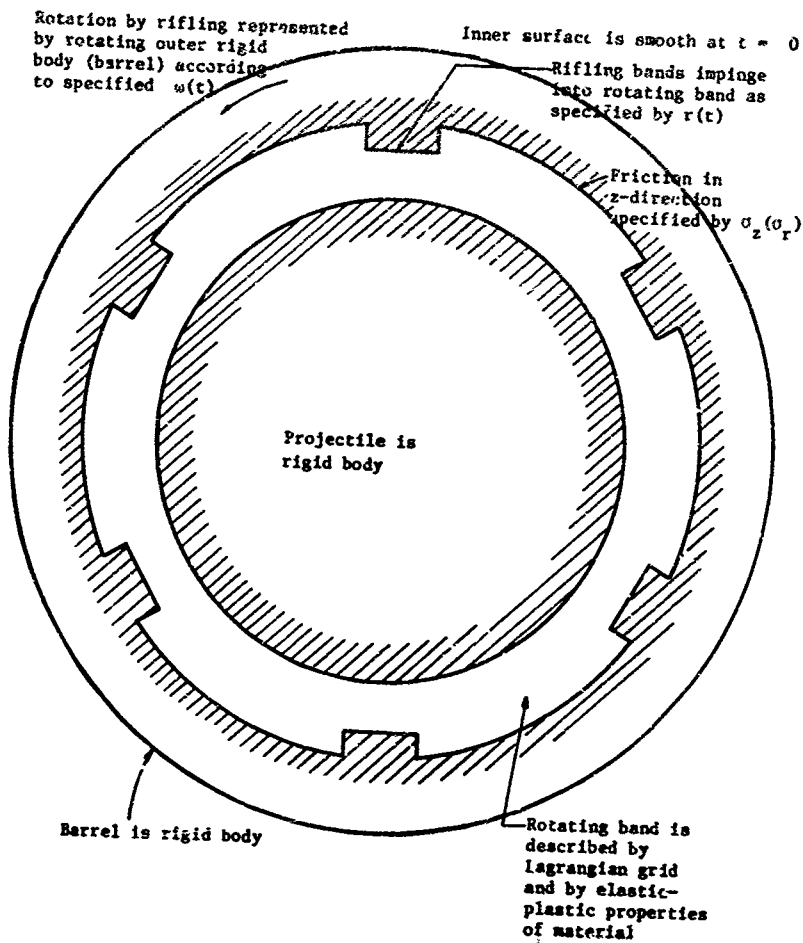


Figure 7. Suggested Method for Plane Strain Analysis of Rotating Band-Rifling Interaction

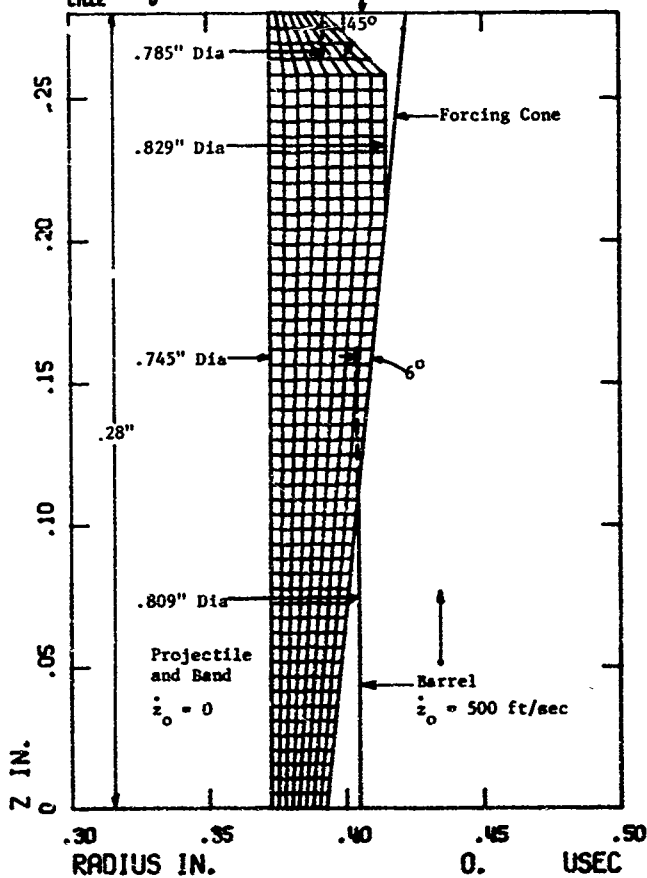


Figure 8. Baseline Plastic Band Geometry and Computational Grid
 (Case 1 and 2 - Baseline Design)

24 JUL 78 CALIFORNIA RESEARCH AND TECHNOLOGY CENTER
SER NO. 3000-3. PLASTIC GRID /CASE INTERACTING
CYCLE 149

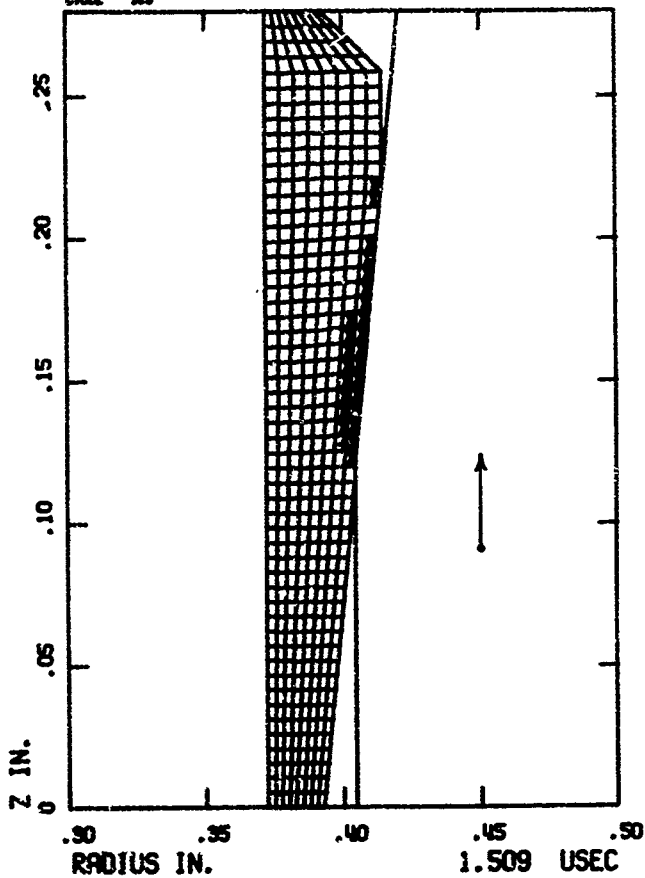


Figure 9. Grid Configuration at 1.5 usec, Case with Friction
(Case 1 - Baseline Design)

21 JUL 78 CALIFORNIA RESEARCH AND TECHNOLOGY MUSEUM CASE
RESEARCH NO. 3010-3. PLASTIC SPRING / CONE INTERACTION
CYCLE 100 UNIT LENGTH = .0000 200 FT/SEC

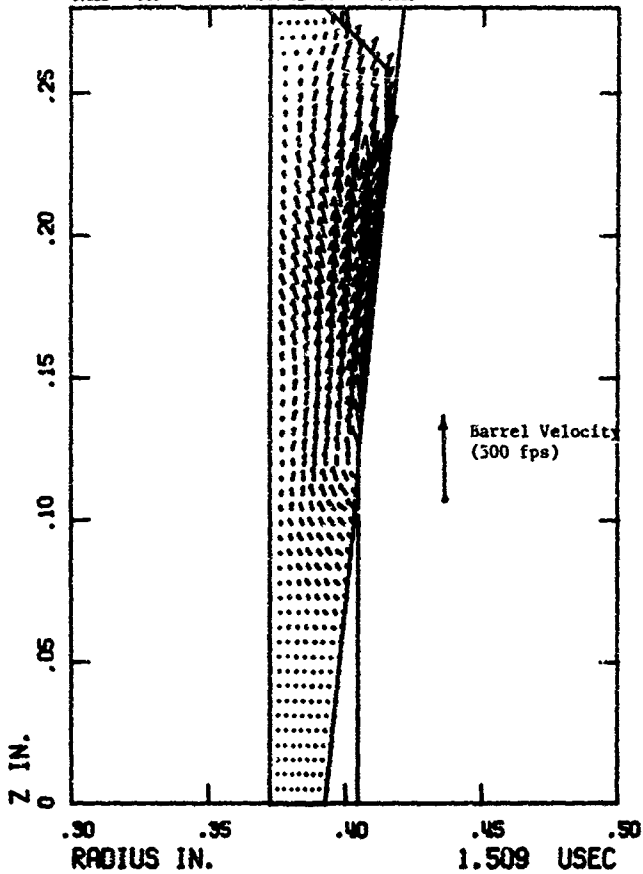


Figure 10. Velocity Field at 1.5 usec, Case with Friction
(Case 1 - Baseline Design)

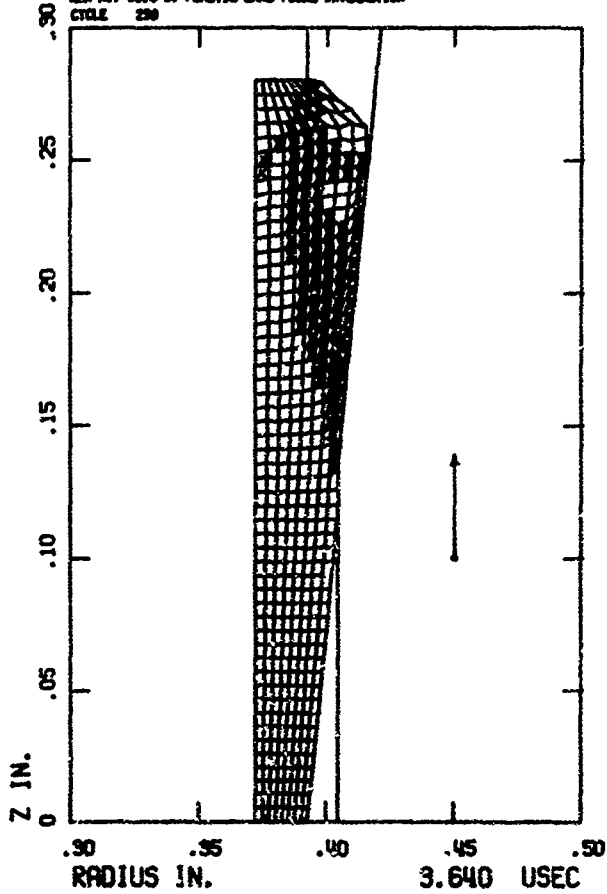


Figure 11. Grid Configuration at 3.6 μ sec, Case with Friction
(Case 1- Baseline Design)

21 JUL 77 CALIFORNIA RESEARCH AND TECHNOLOGY CENTER
 SAN DIEGO 92161-5000 PLASTIC BARRIERS / CYCLES INTERACTION 250 FT/SEC
 CYCLE 200 NET LENGTH = .3000

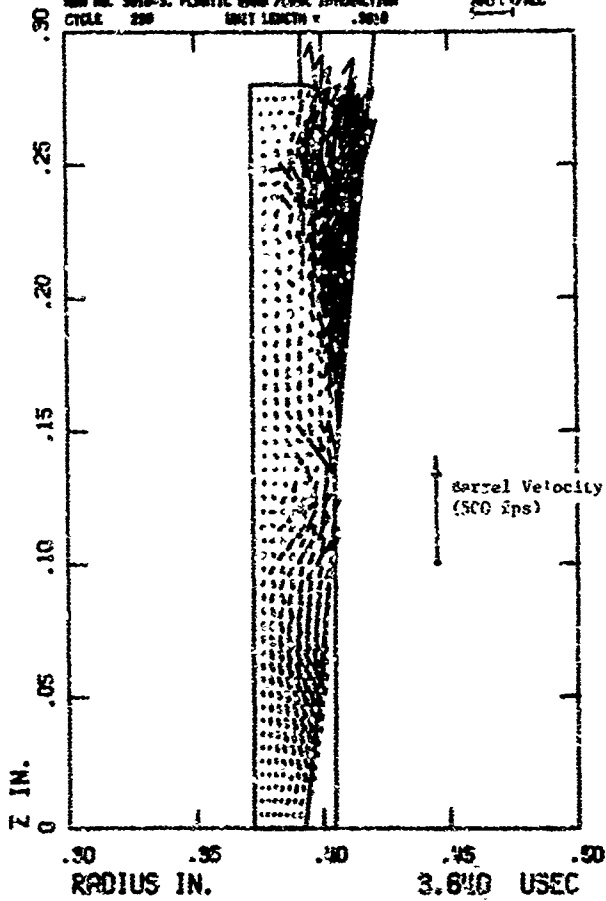


Figure 12. velocity Field at 3.6 μ sec, Case with Friction
 (Case 1-Baseline Design)

GM 800 75 CALIFORNIA RESEARCH AND TECHNOLOGY CENTER
 SAN DIEGO, CALIF. 92161-5000
 CYCLE 105 UNIT LENGTH = .1005 200 FT/SEC

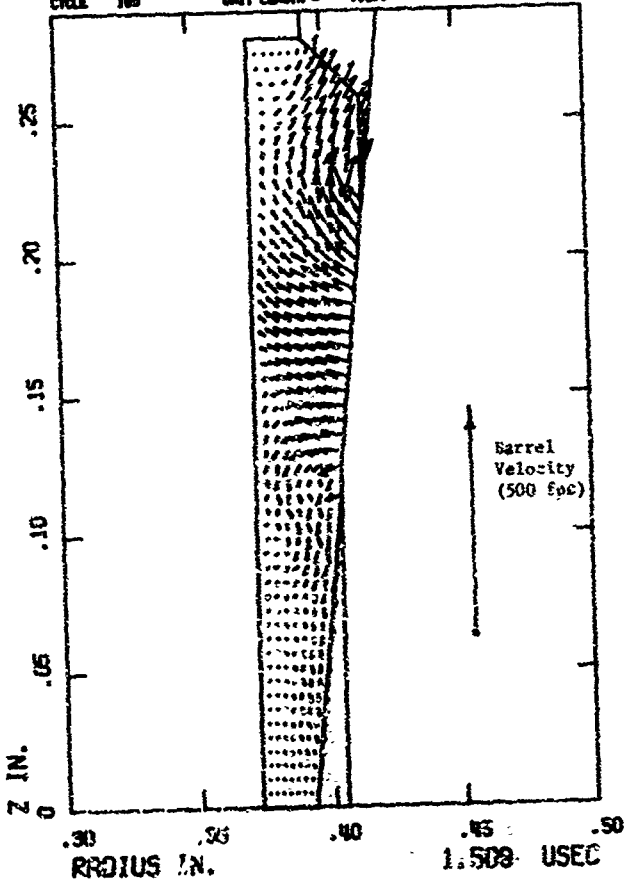


Figure 13. Velocity Field at 1.5 usec, Case without Friction
 (Case 2-Baseline Design)

DA AGO 75 CALIFORNIA RESEARCH AND TECHNOLOGY CENTER
 MEM. NO. 3048-2. PLASTIC BLOWING INTERACTION
 CYCLE 200

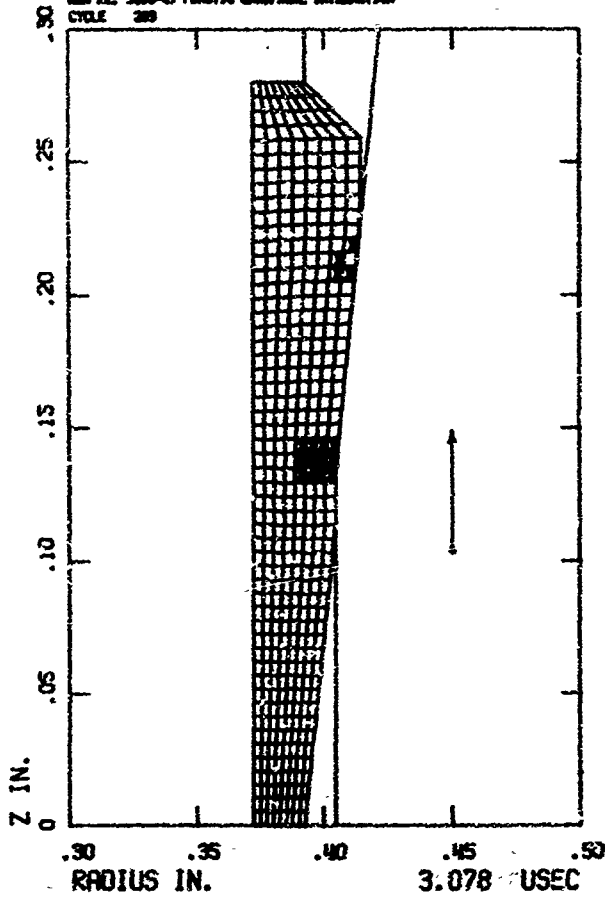


Figure 14: Grid Configuration at 3.1 usec, Case without Friction (Case 2-Baseline Design)

CALIFORNIA RESEARCH AND TECHNOLOGY CENTER, UNIVERSITY OF CALIFORNIA, SAN DIEGO, CALIF. 92162

68 888 75 CALIFORNIA RESEARCH INC VERMILION 9084-1 042
 801 88 3810-4 PLASTIC SPRING/CRACK INVESTIG
 COLE 200 UNIT LEVER = .100 200 FT/SEC

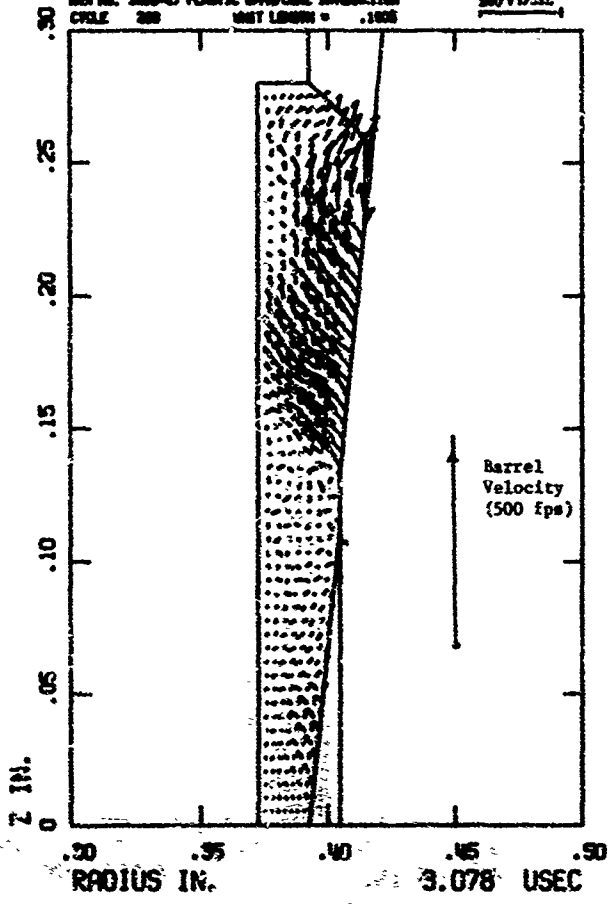


Figure 15. Velocity Field at 3.1 usec. Case without Friction.
 (Case 2-Baseline Design).

60 AND 75 CALIFORNIA RESEARCH AND TECHNOLOGY WING-L CASE
REM NO. 3000-L PLASTIC SHOCKWAVE IMPROVED IMPROVED
CYCLE 307

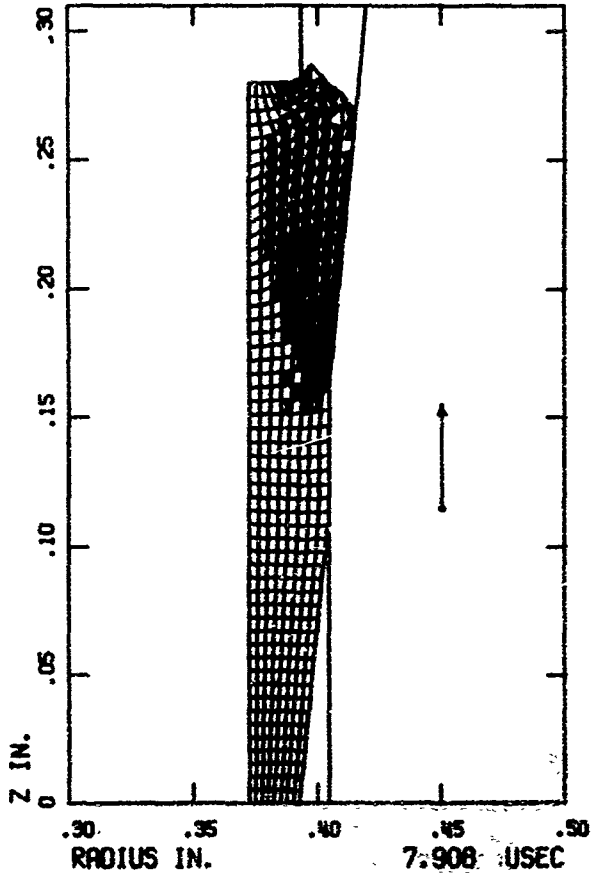


Figure 16. Grid Configuration at 7.9 μ sec, Case without Friction
(Case 2 - Baseline Design)

80 AND 75 CALIFORNIA RESEARCH AND TECHNOLOGY MFG-C CASE
 800 02. 3000-L PLASTIC SHEETING INJECTION
 CYCLE 907 UNIT LENGTH = .7520

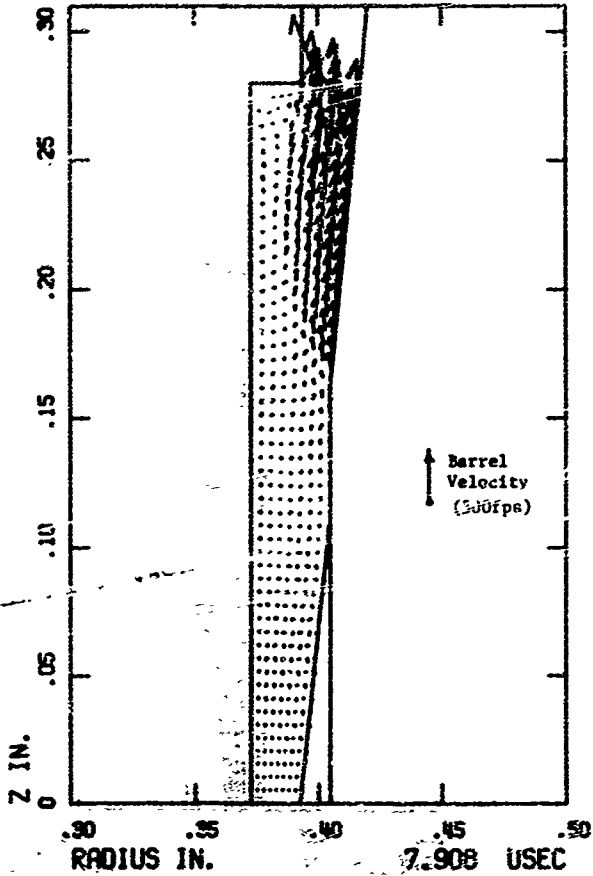


Figure 17. Velocity Field at 7.9 usec, Case without Friction
 (Case 2 - Baseline Design)

30 SEP 75 CALIFORNIA BOMBARDIER AND TECHNOLOGY NEWS-L CORP
 GEN. NO. 3000-A. PLASTIC SHEET/PIPE PRODUCTION (FRCTIONLESS)
 CYCLE 00

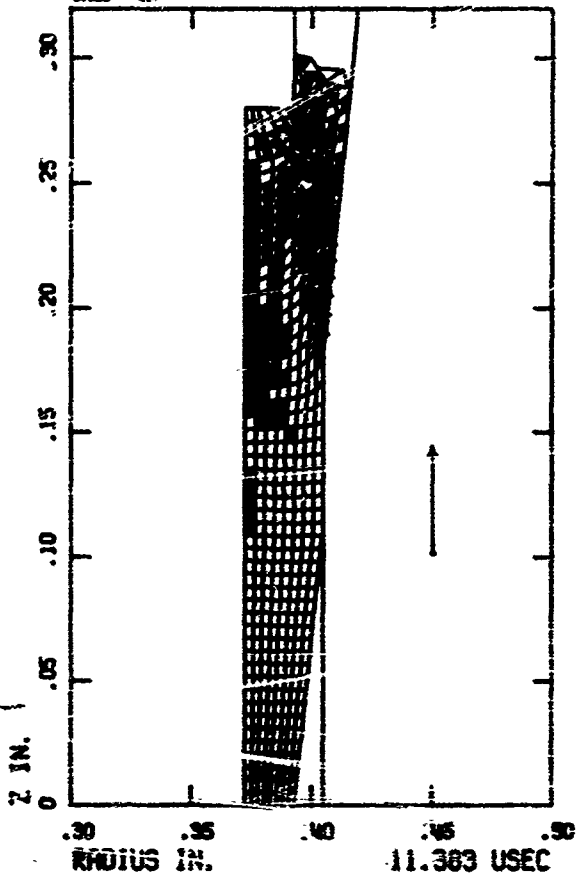


Figure 18. Grid Configuration at 11.4 usec, Case without Friction
 (Case Z - Baseline Design)

30 SEP 75 CALIFORNIA BOMBARDIER AND TECHNOLOGY NEWS-L CORP GEN. NO. 3000-A. PLASTIC SHEET/PIPE PRODUCTION (FRCTIONLESS) CYCLE 00

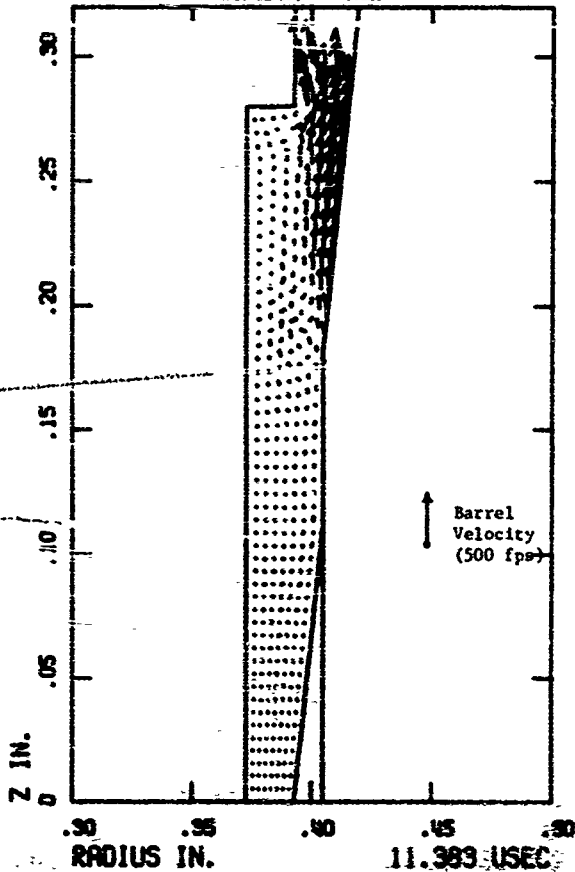


Figure 19. Velocity Field at 11.4 usec. Case Without Friction (Case 2 - Baseline Design)

11 SEP 75 CALIFORNIA RESEARCH AND TECHNOLOGY CENTER
 REP. NO. 7500-2. PLASTIC BEAD/CRACK INTERACTION STUDIES
 VOL. 007

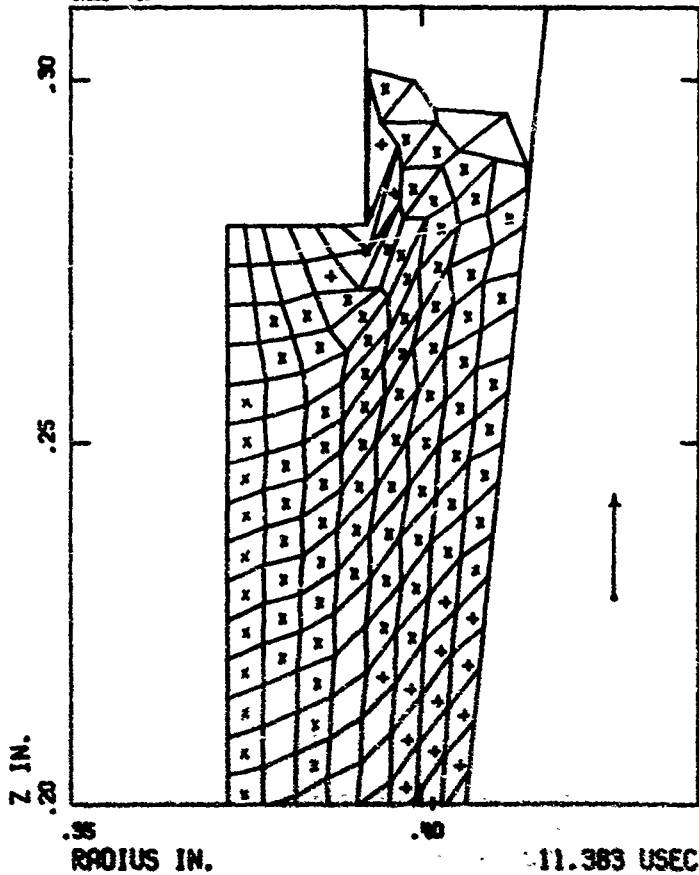


Figure 20. Grid Configuration at Rear Section of Plastic Bead at 11.4 μ sec,
 Case without Friction (Case 2 - Baseline Design)

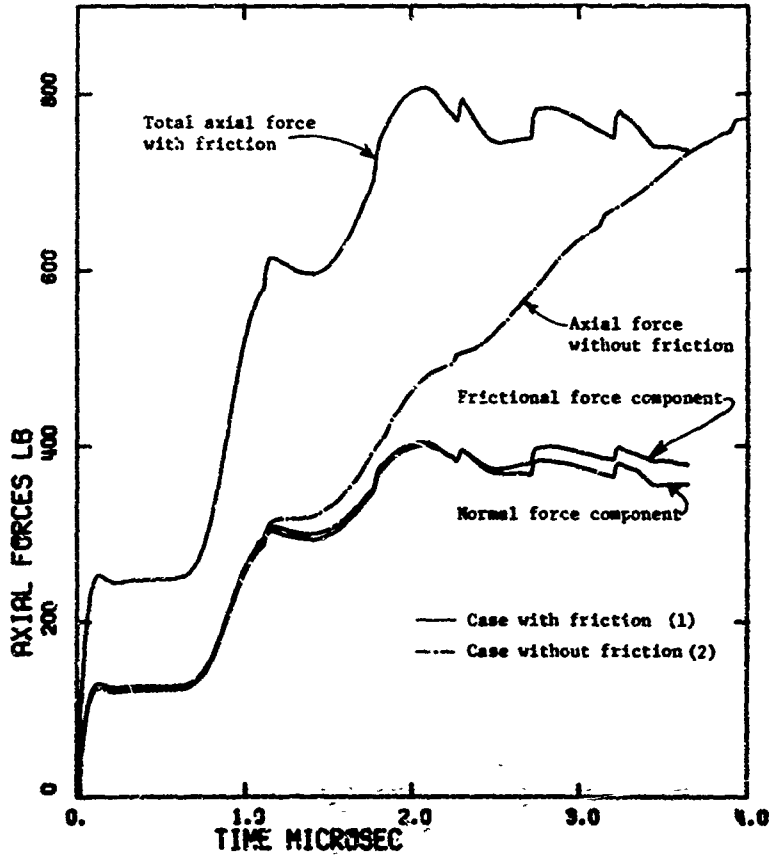


Figure 21. Comparison of Axial Forces on Borel with and without Surface Friction (Cases 1 and 2 - Baseline Design)

CALIFORNIA RESEARCH AND TECHNOLOGY, INC.

RUN NO. 2810-3, PLASTIC BARREL/CONE INTERACTION

01 AUG 75

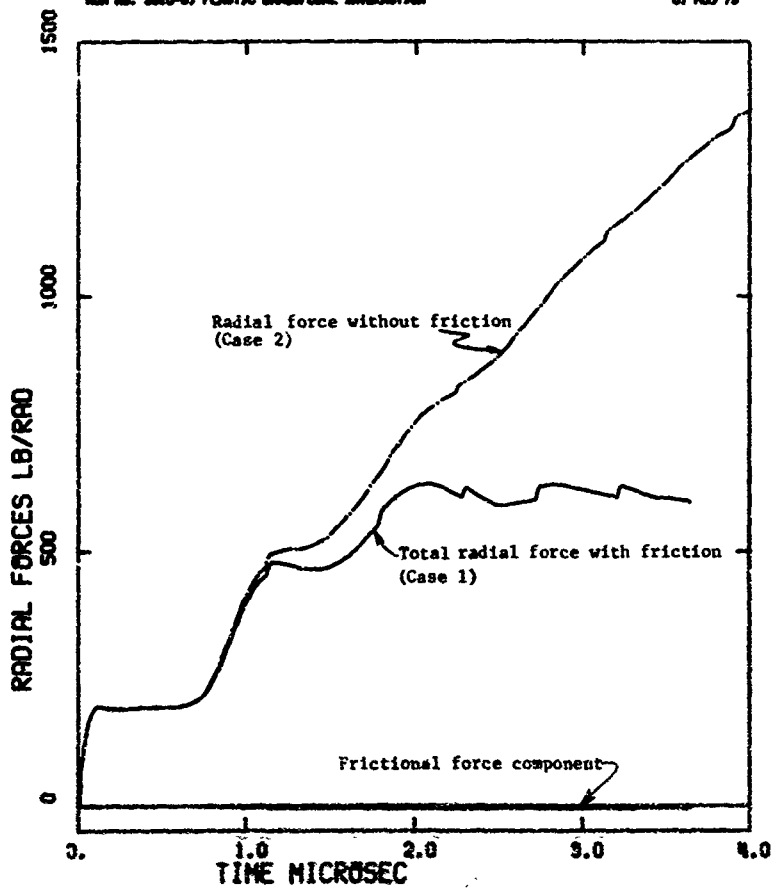


Figure 22. Comparison of Radial Forces on Barrel with and without Surface Friction (Cases 1 and 2 - Baseline Design)

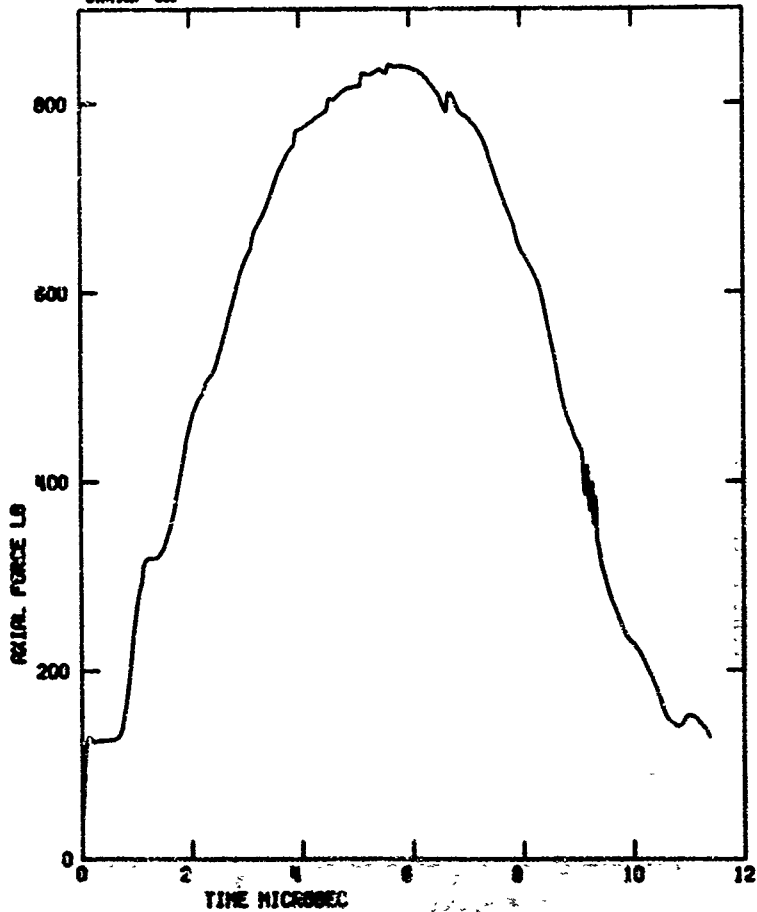


Figure 23. Axial Force at Band/Barrel Interface vs Time, Case without Friction (Case 2 - Baseline Design)

CALIFORNIA RESEARCH AND TECHNOLOGY, INC.
5001 MI. 5000-L PLASTIC CONDENSED EXPANSION (FRAGMENTARY)
CONTINUED 300

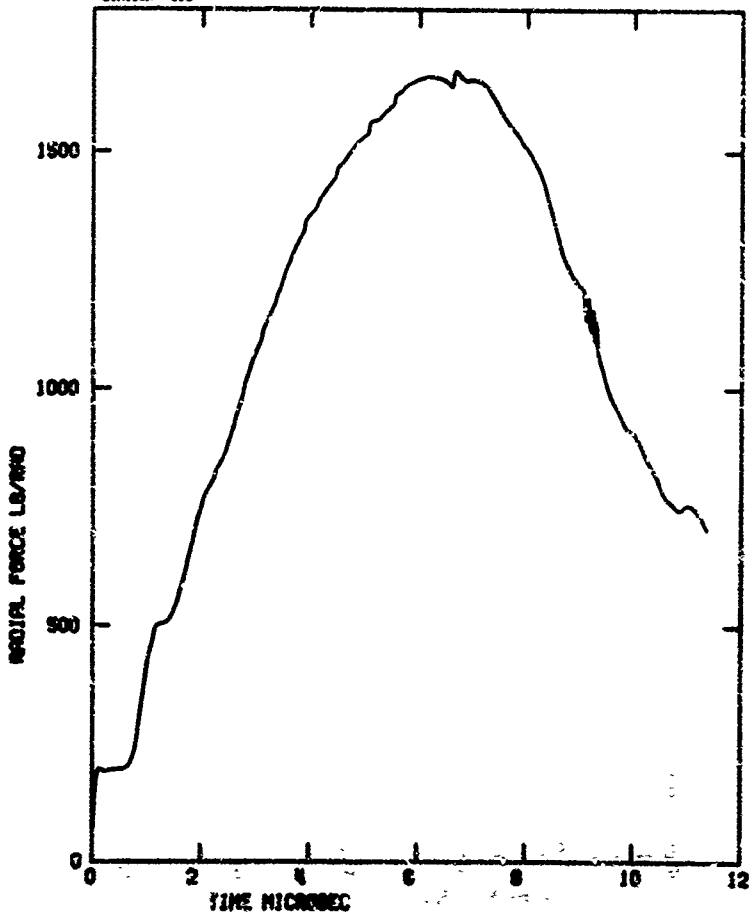


Figure 24. Radial Force at Band/Barrel Interface vs Time, Case without Friction (Case 2 - Baseline Design)

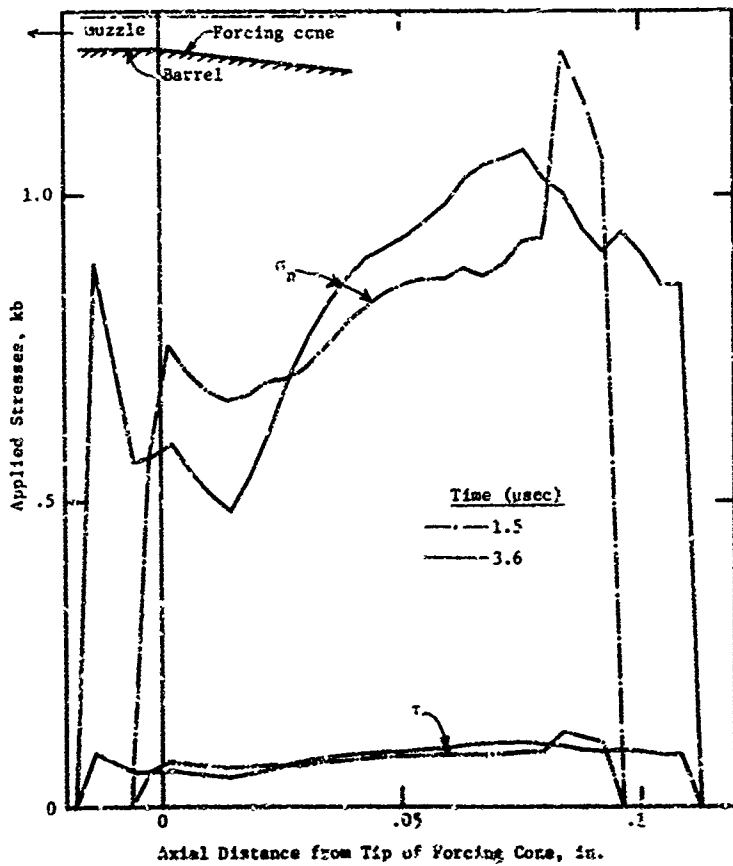


Figure 25. Normal Stress (σ_n) and Tangential Stress (τ) Distributions on Barrel. Case with Friction (Case 1 - Baseline Design)

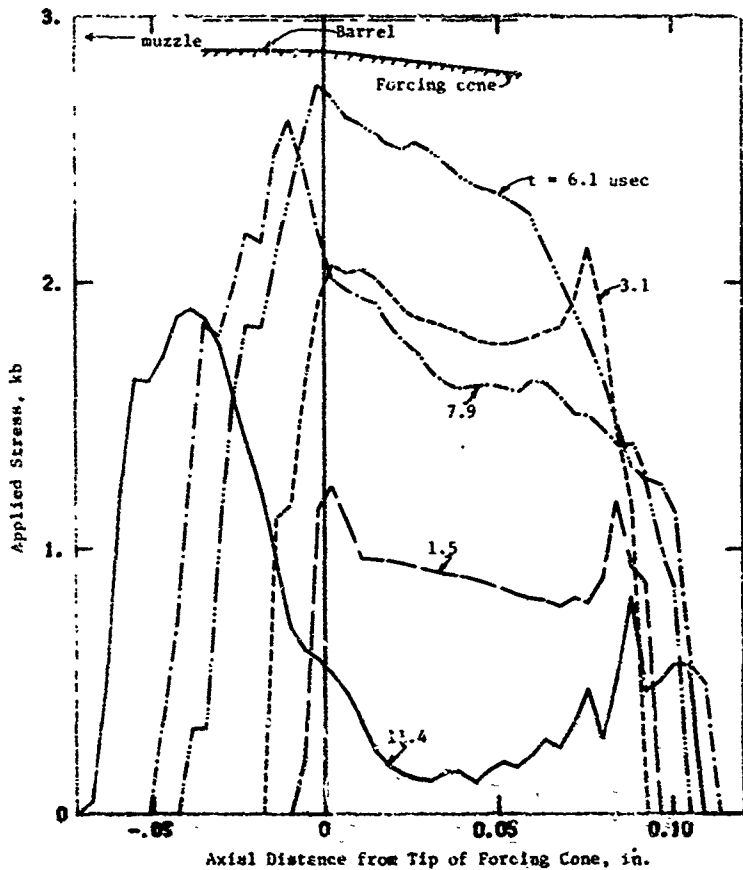


Figure 26. Normal Stress (σ_x) Distributions on Barrel, Case without Friction (Case 2 - Baseline Design).

11 SEP 78 CALIFORNIA EXPLOSION AND TECHNOLOGY CENTER
 200 DR. 200-8 PLASTIC BAND/PLATE STRUCTURE
 CASE 3

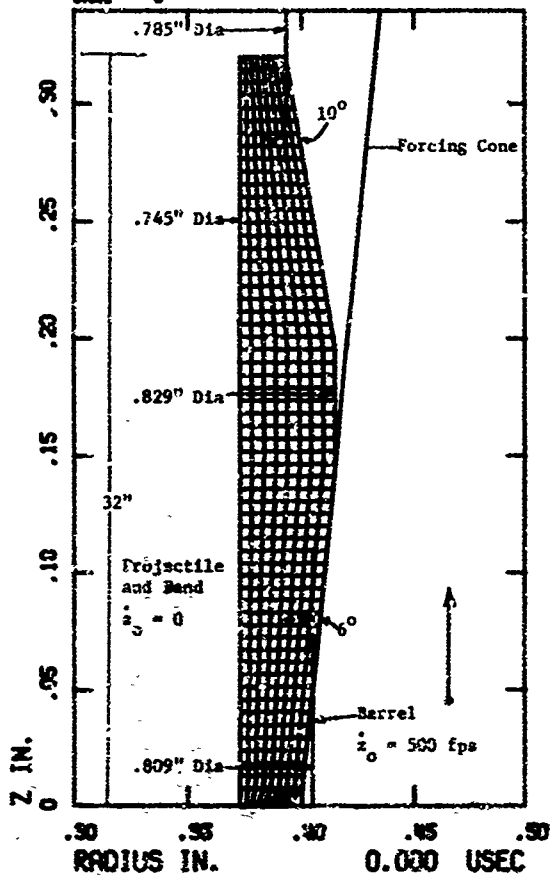


Figure 27. Modified Plastic Band Geometry, and Computational Grid
 (Case 3 - Modified Design)

18 SEP 75 CALIFORNIA RESEARCH AND TELEVISION NEWS-L. PAGE
REV. NO. 3430-6. PLASTIC SAND/ORE INTERACTION
CYCLE 300

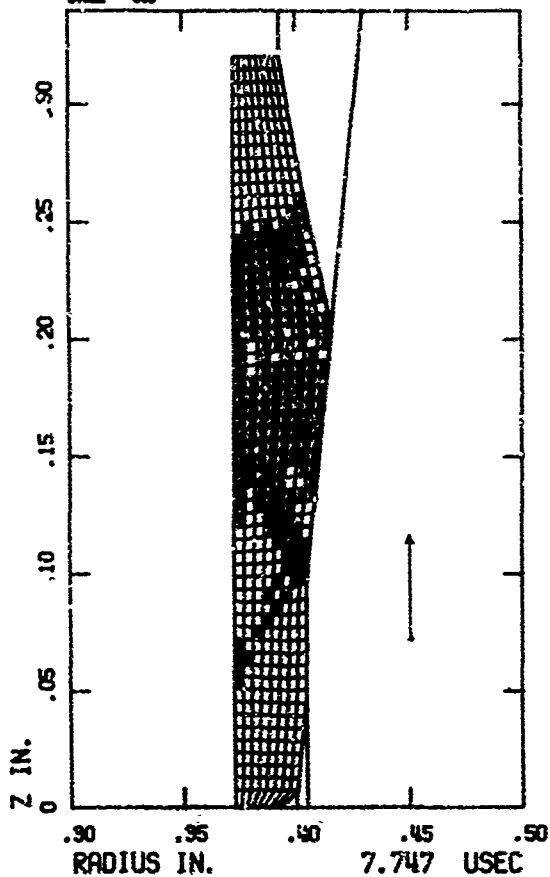


Figure 28. Grid Configuration at 7.7 usec, Modified Plastic Sand Design
(Case 3)

30 SEP 78 04:50PM RICHMOND AIR TERMINAL WVA-1 CASE
 FOR NO. 2025-2. PLASTIC BOND/CASE SEPARATION 200 F/SEC
 CYCLE 000 NEXT LENGTH = .2000

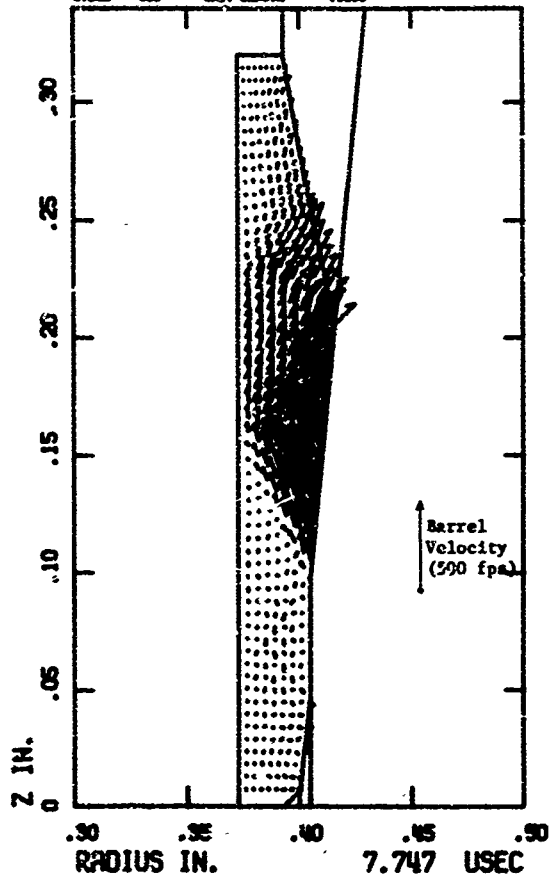


Figure 29. Velocity Field at 7.7 usec, Modified Plastic Bond Design
 (Case 3)

30 82-78 CHLORINE RESERVE AND TECHNOLOGY WING-1. CASE
SER. NO. 2000-6. PLASTIC BAND-DRIVE INDUSTRY:
CYCLE 128

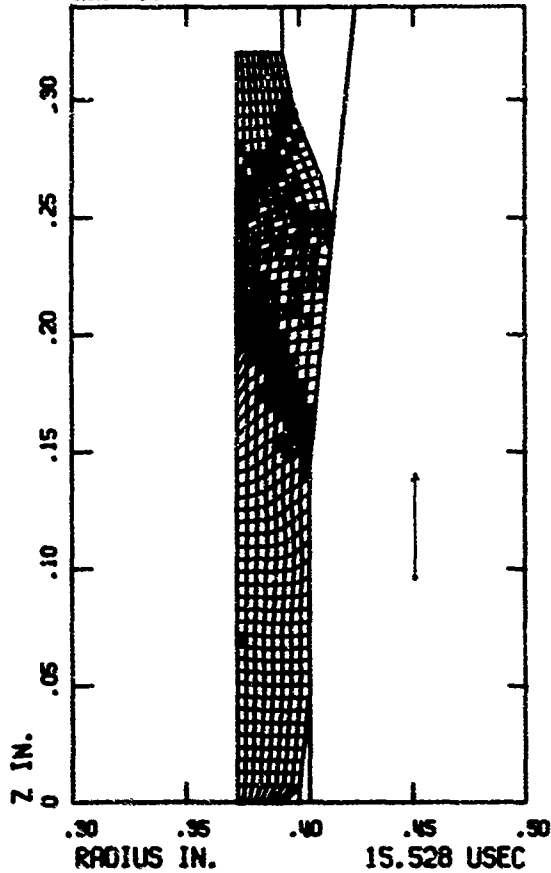


Figure 30. Grid Configuration at 15.5 usec, Modified Plastic Band Design
(Case 3)

20 SEP 78 CALIFORNIA RESEARCH AND TECHNOLOGY IMPV-L OSC
SER NO. 3000-G. PLASTIC STRUCTURE RESISTIVITY
CYLE 1000

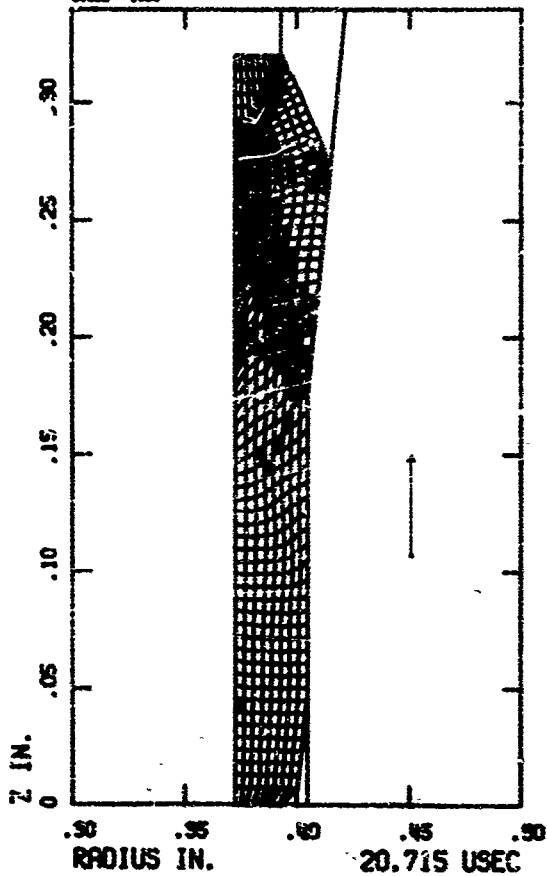


Figure 31. Grid Configuration at 20.7 usec, Modified Plastic Band Design (Case 3)

21 SEP 78 CALIFORNIA RESEARCH AND TECHNOLOGY MFG-L CODE
REV. 02, 1969-S. PLASTIC INFLUENCE INTERACTION
FILE 2222

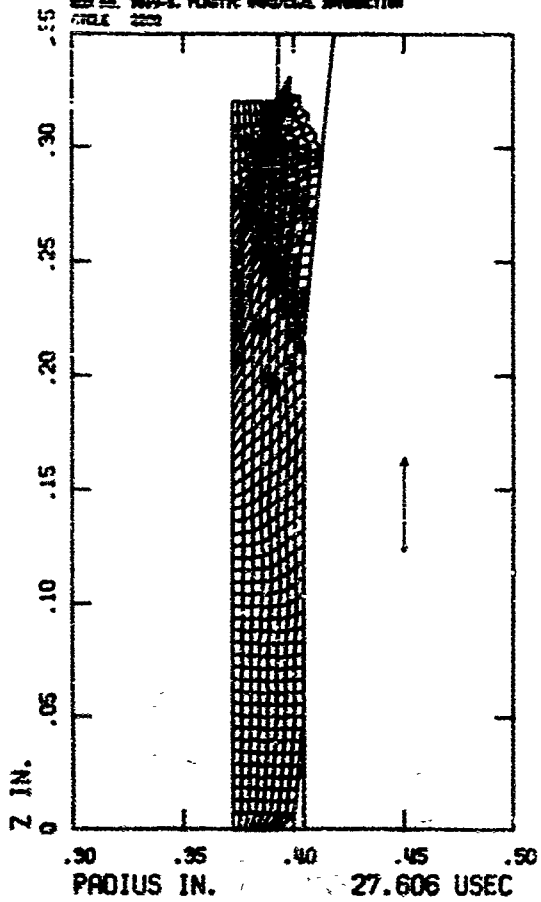


Figure 32. Grid Configuration at 27.6 μ sec, Modified Plastic Band Design (Case 3)

21 SEP 75 CALIFORNIA ELECTRONIC TECHNOLOGY CENTER
 REP. NO. 7506-2. PLASTIC BOND/PIPE ANALYSIS FOR PL/SEC
 CYCLE 2000 UNIT LENGTH = .0072

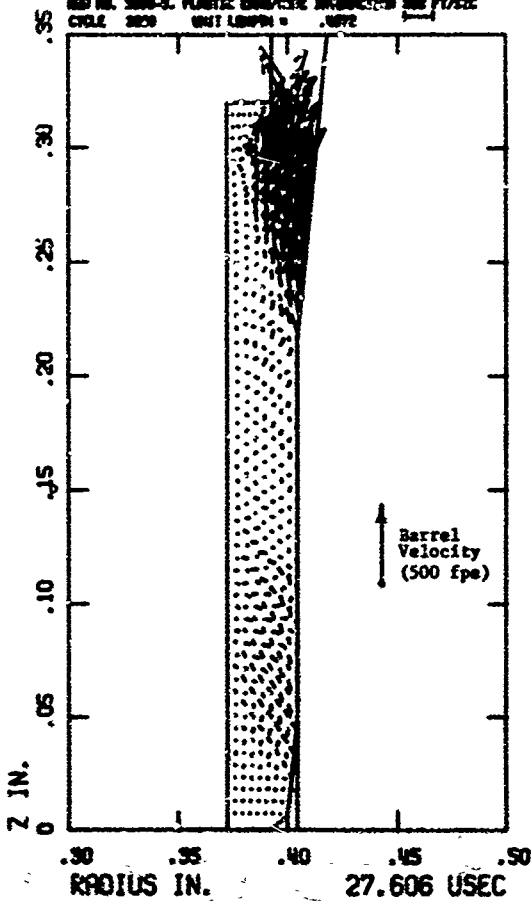


Figure 33. Velocity Field at 27.6 usec, Modified Plastic Bend Design (Case 3)

CALIFORNIA RESEARCH AND TECHNOLOGY, INC.
3000 W. 20th ST. PLATEAU GUN/CORE INTERFACES
SUTHER 000

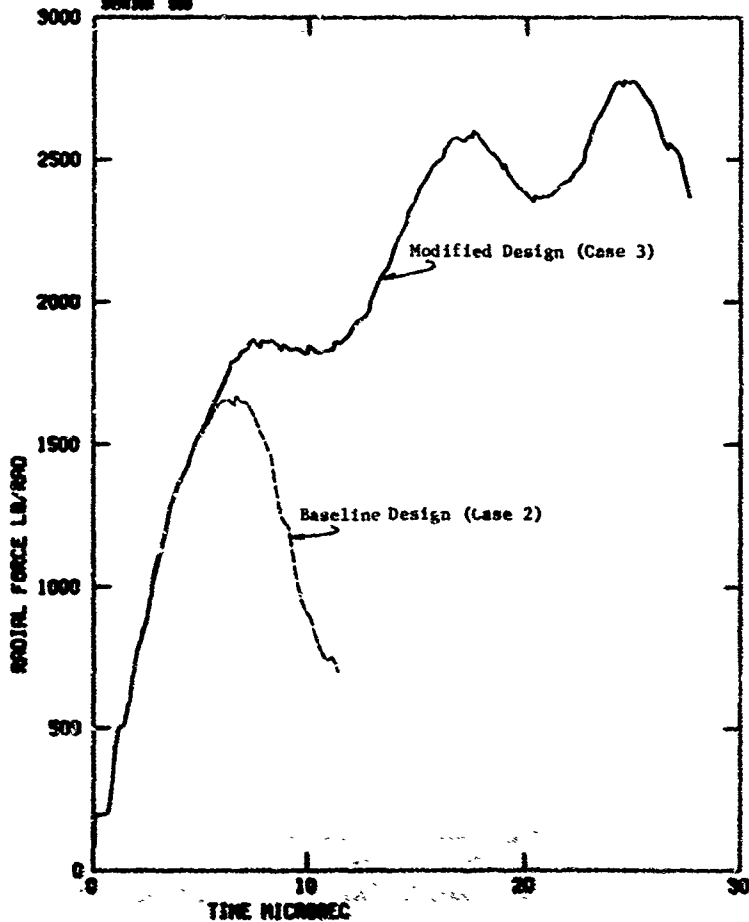


Figure 34. Radial Force at Base/Barrel Interface vs Time for Baseline and Modified Plastic Head Designs

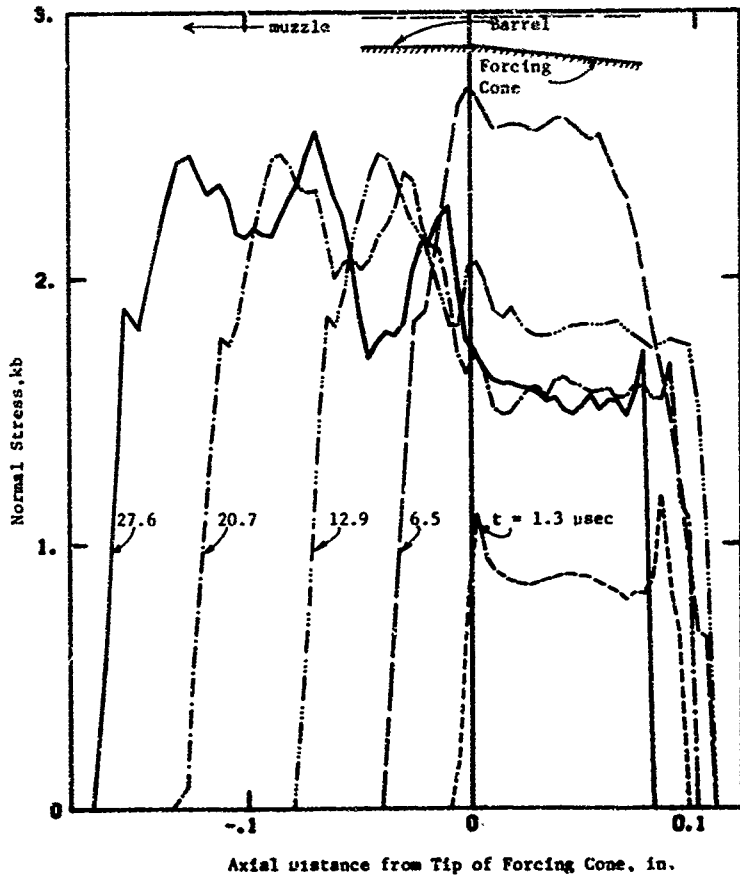


Figure 35. Distributions of Normal Stress along Band/Barrel Interface, Modified Plastic Band Design

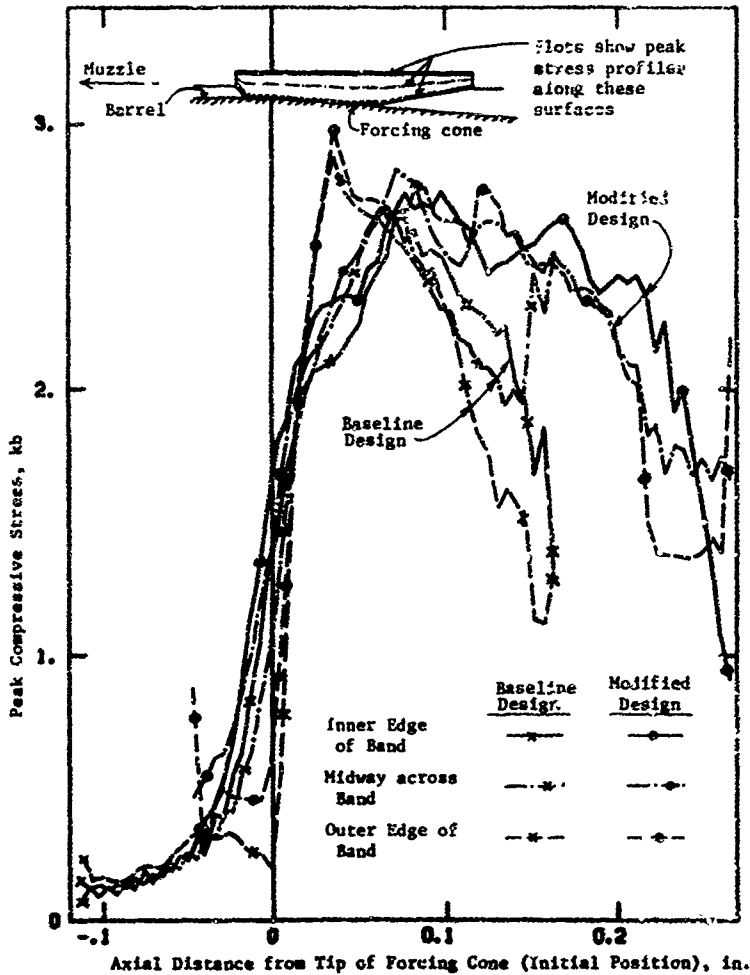


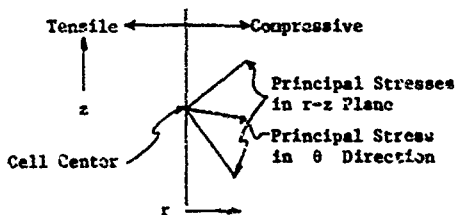
Figure 36. Peak Compressive Stresses within Band; Baseline and Modified Plastic Band Designs (Cases 2 and 3)

FD-302 (Rev. 1-25-60)

APPENDIX A
PRINCIPAL STRESS FIELD PLOTS

In addition to the plots of the grid configuration and the velocity field presented in Section II of the report, plots of the principal stress field occurring at several times during each of the solutions were obtained. A representative selection of these for Cases 1, 2, and 3 are contained in this Appendix.

In the stress field plots, the principal components of the stress tensor for each cell are shown as follows: The magnitude of the two principal stresses in the r - z plane are plotted in their corresponding principal directions. The third principal stress (in the azimuthal direction) is plotted along the line bisecting the other two principal directions. Vectors pointed to the right are compressive, to the left, tensile. An example of how a stress tensor is plotted is sketched below:



The scale of the stress vectors is given at the top of each plot. The plots listed below are given in the following set of figures:

Case 1:	1.5, 3.5 μ sec
Case 2:	2.1, 7.9, 11.4 μ sec
Case 3:	7.7, 15.5, 27.6 μ sec

91 JUL 75 CALIFORNIA RESEARCH AND TECHNOLOGY MUSEUM CODE
 RWB NO. 3019-S. PLASTIC STRESS / ZONE INTERACTION
 CYCLE 100 UNIT LENGTH = .1000 1 KB

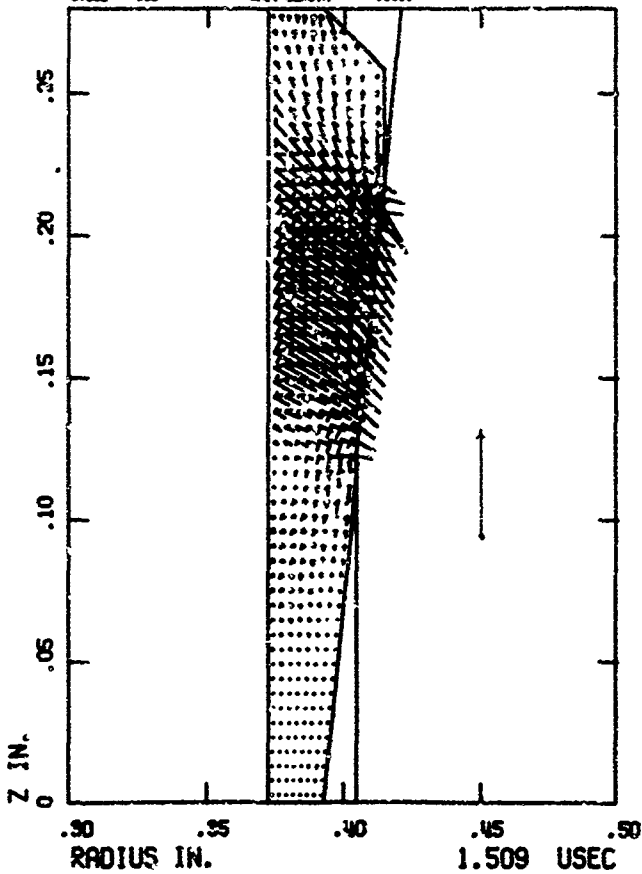


Figure A-1. Principal Stress Field at 1.5 usec, Case with Friction (Case 1 - Baseline Design)

31 JAN 75 CALIFORNIA RESEARCH AND TECHNOLOGY MFG-L CRCE
 RES NO. 3018-3. PLASTIC BOND /CONE INTERACTION
 CYCLE 230 UNIT LENGTH 0 .1018

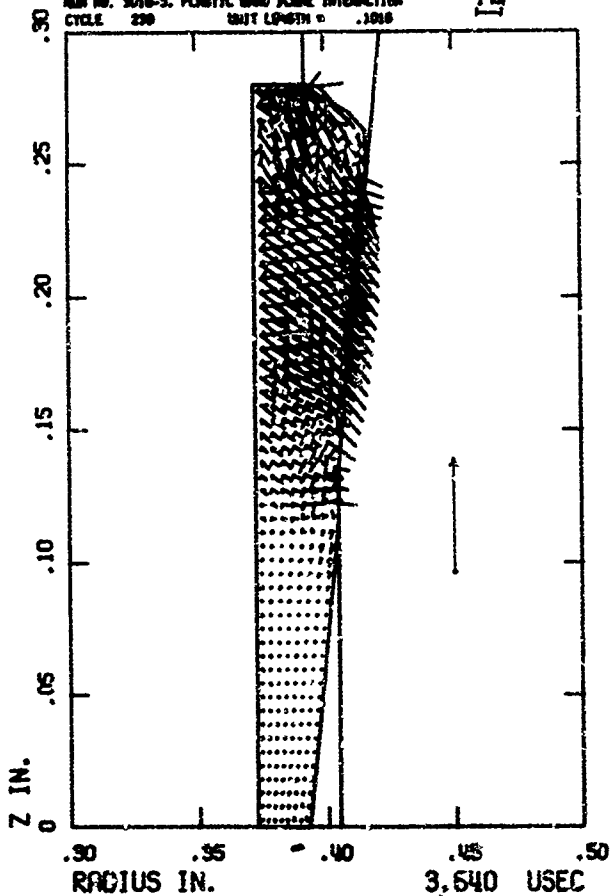


Figure A-2. Principal Stress Field at 3.6 usec, Case with Friction (Case 1 - Baseline Design)

OS 88-75 CALIFORNIA RESEARCH AND TECHNOLOGY MINE-L. ONE
RAN NO. 3010-A. PLASTIC SHEAR/CONE INTERACTION
CYCLE 200 UNIT LENGTH = .1275

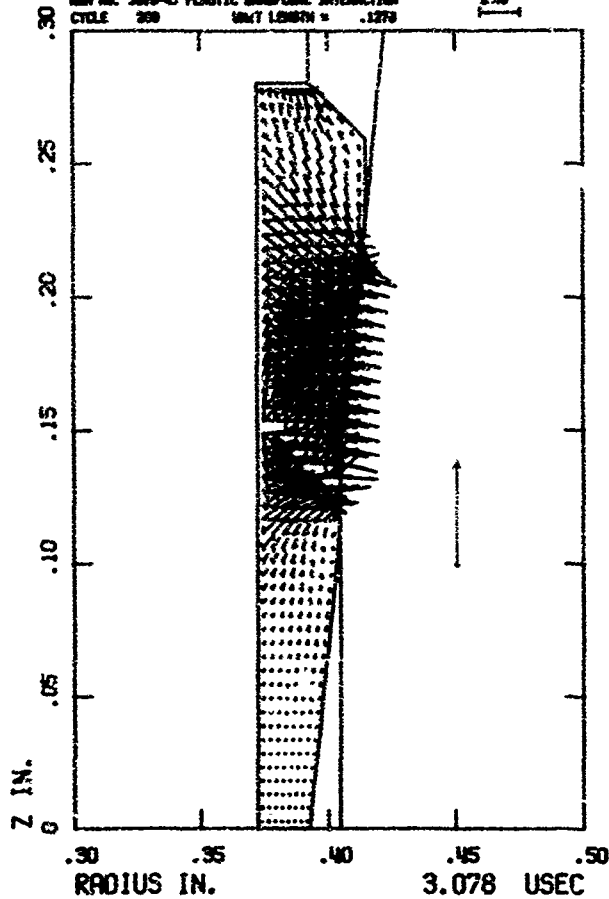


Figure A-3. Principal Stress Field at 3.1 usec, Case without Friction
(Case 2 - Baseline Design)

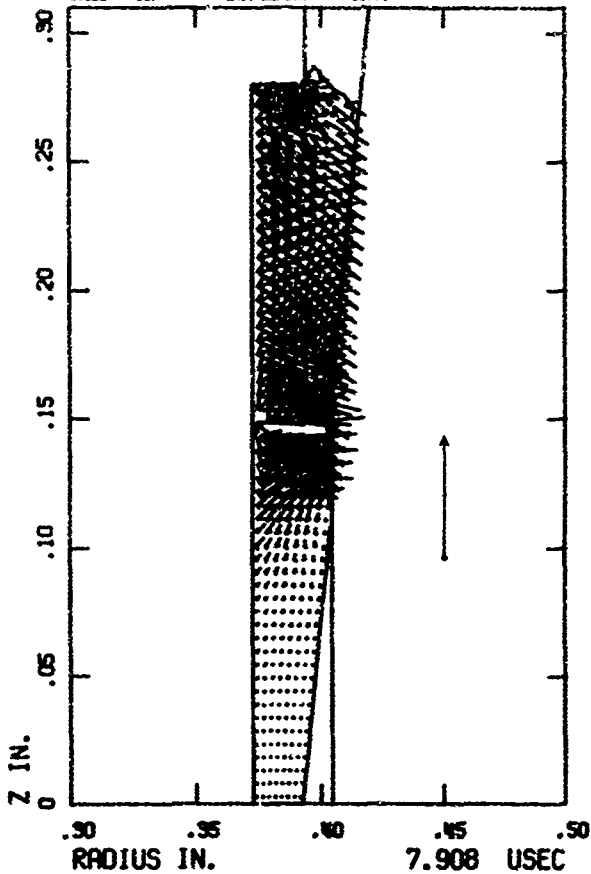


Figure A-4. Principal Stress Field at 7.9 usec, Case without Friction
 (Case 2 - Baseline Design)

20 SEP 75 CALIFORNIA RESEARCH AND TECHNOLOGY MUSE-L CODE
 CASE NO. 3000-L PLASTIC BUCKLING BUBBLES/SHOCK 2 KC
 CYCLE 009 UNIT LENGTH = .1776

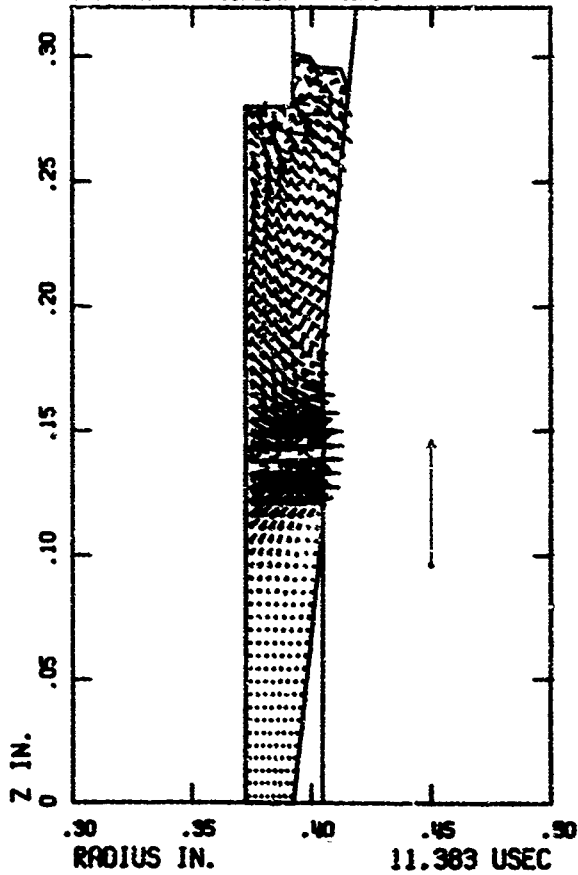


Figure A-5. Principal Stress Field at 11.4 usec, Case without Friction
 (Case 2 - Baseline Design)

25 SEP 75 CALIFORNIA RESEARCH AND TECHNOLOGY INVE-1 CORP
 DRG NO. 2010-6. PLASTIC BOND/CONE IMPROVED 3 22
 CYCLE 000 UNIT LENGTH = .2500

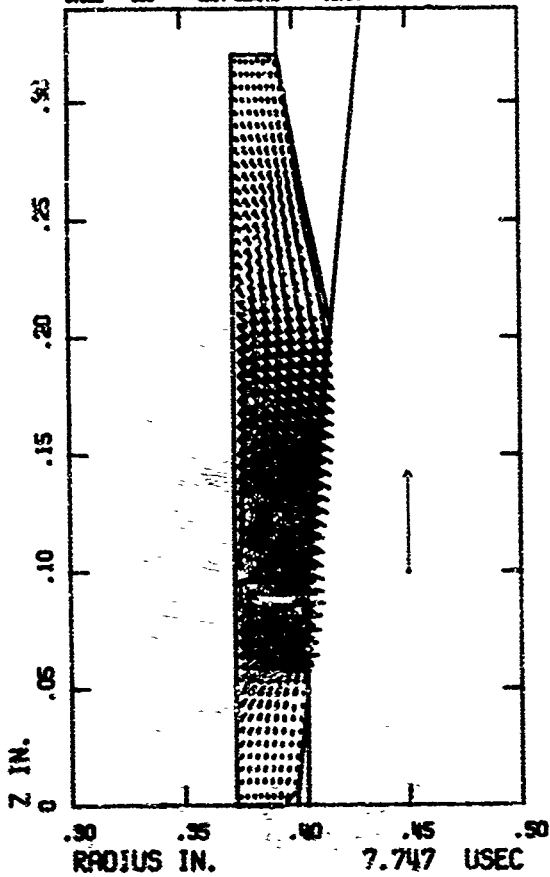


Figure A-6. Principal Stress Field at 7.7 usec, Modified Plastic Band Design
 (Case 3)

16 SEP 75 CALIFORNIA UNIVERSITY SAN DIEGO UNIV. CALIF.
 SDI NO. 3000-2. PLASTIC SPREADING IMPROVED 3 1/2
 CYCLE 1000 UNIT LENGTH = .200

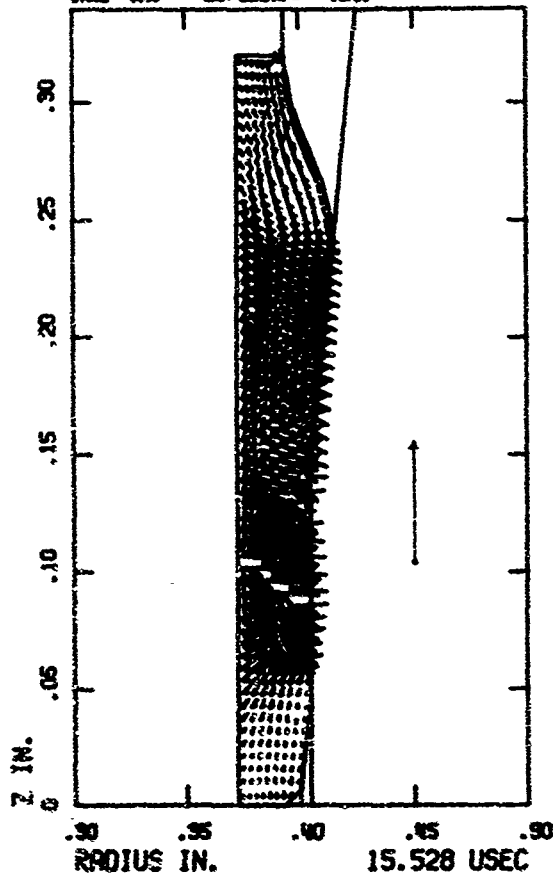


Figure A-7. Principal Stress Field at 15.5 usec, Modified Plastic Band Design (Case 3)

21 SEP 75 CALIFORNIA RESEARCH AND TECHNOLOGY MWP-L CODE
SER. NO. 3010-5. PLASTIC BAND-CLASH INTERACTION 3 KB
CYCLE 2308 UNIT LENGTH = .2704

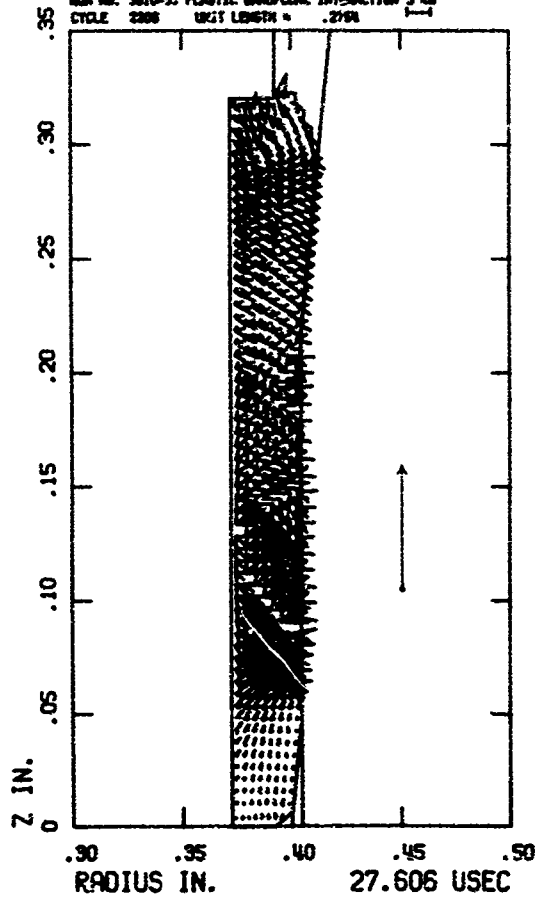


Figure A-8. Principal Stress Field at 27.6 usec, Modified Plastic Band Design (Case 3)

APPENDIX B

TIME HISTORIES OF STRESS AND VELOCITY

Parameter-time histories were recorded at several locations in the plastic band. The locations of the stations are shown in Figure B-1 for Cases 1 and 2 and in Figure B-2 for Case 3. The stations for Case 3 were placed at analogous positions to those used in the first design so that the response of the two bands could be compared. The following parameters are plotted:

- a. Radial stress σ_r
- Axi stress σ_z
- Hoop stress σ_θ
- Shear stress σ_{rz}

- b. Radial particle velocity \dot{r}
- Axial particle velocity \dot{z}

Positive stresses are compressive. Positive \dot{r} is radially outward. Positive \dot{z} is axially upward (in the direction of the barrel velocity).

The first set of figures (B-3 to B-9) are comparative plots of the response for Cases 1 and 2 (the basic plastic band geometry with and without friction) at selected stations. The previously noted "locking-on" of the surface of the band to the barrel due to friction during the Case 1 solution is clearly shown in Figure B-3, the velocity plot at Station 8. The second set of figures (B-10 to B-19) are comparative plots from Cases 2 and 3 (the basic and modified plastic band geometry). Note that the extrusion action that occurred at Station 9 in the original design did not occur with the revised design (Figure B-19).

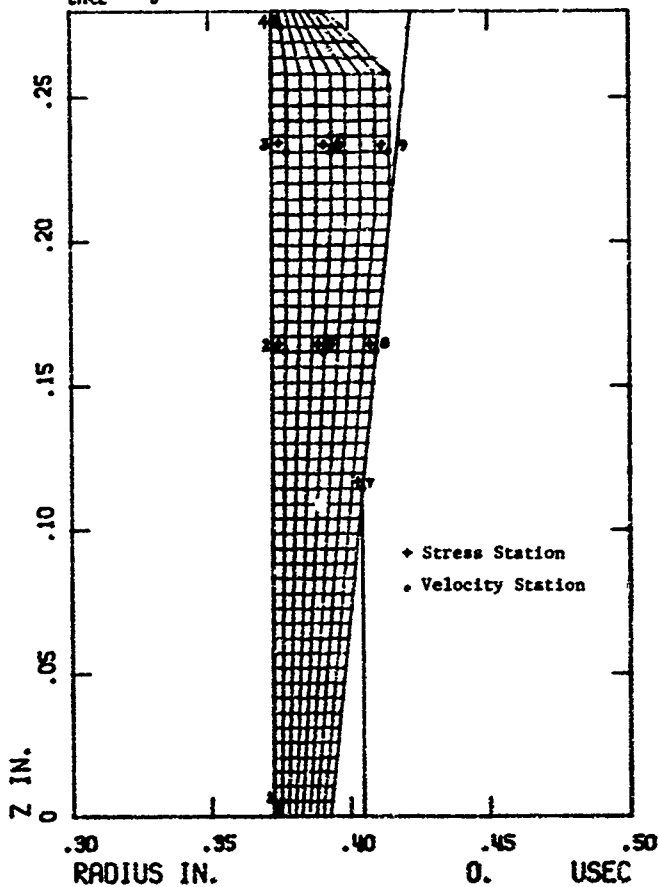


Figure B-1. Locations of Parameter-Time Stations (Cases 1 and 2-Baseline Design)

11 SEP 75 CALIFORNIA REGIONAL AND TECHNOLOGY CENTER CODE
 RM 15. 3010-5. PLASTIC COLLISION INTERACTION
 CYCLE 0

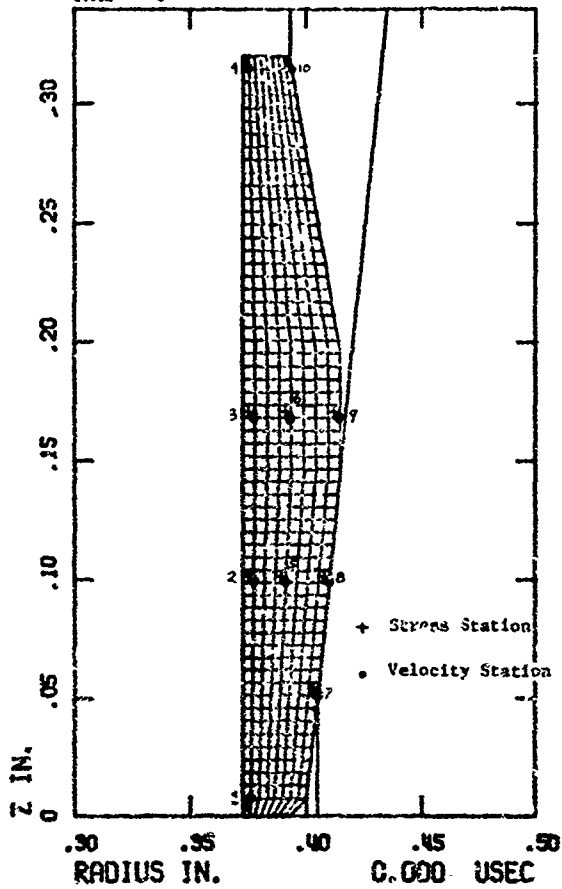


Figure B-2. Locations of Parameter-Time Stations, Modified Plastic Case Design (Case 3)

FROM: https://www.industrydocuments.ucsf.edu/docs/1192

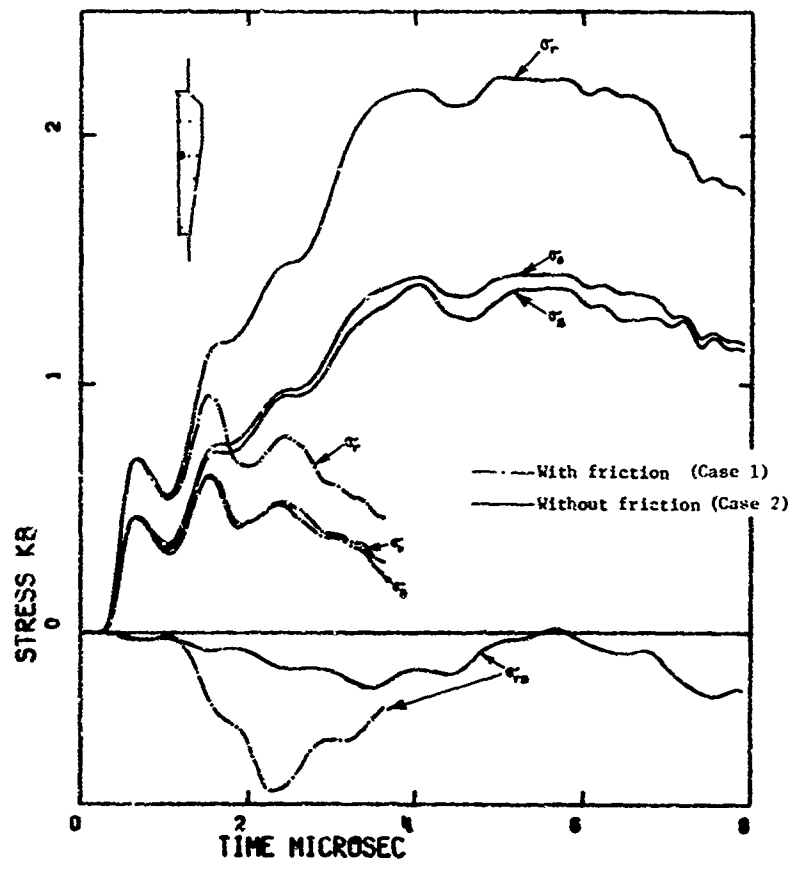


Figure B-3. Stress Components at Station 2 - Baseline Design

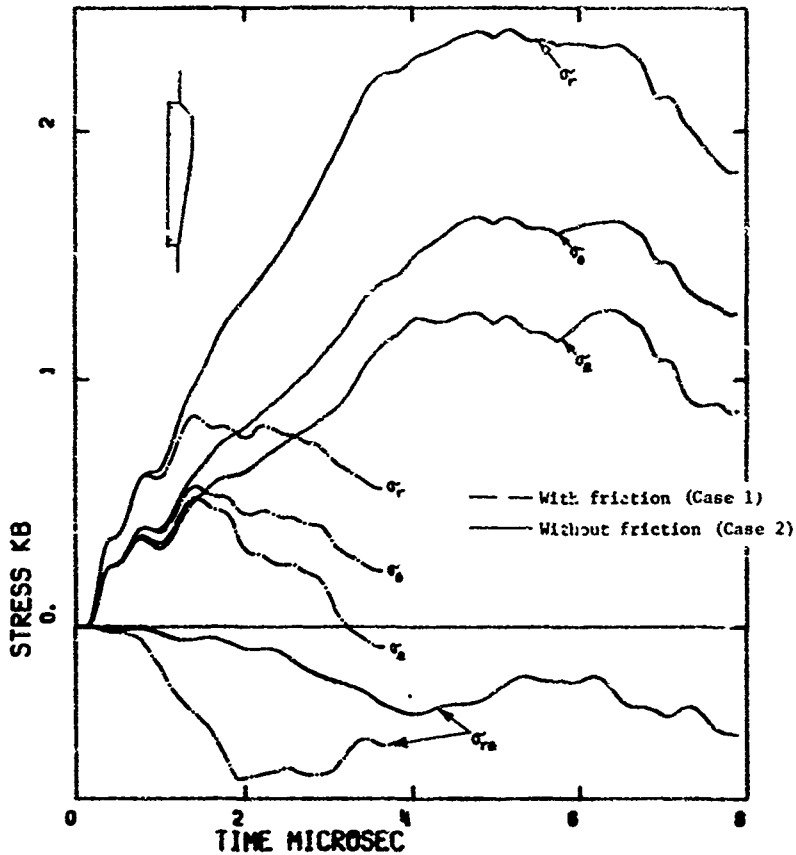


Figure B-4. Stress Components at Station 5 - Baseline Design

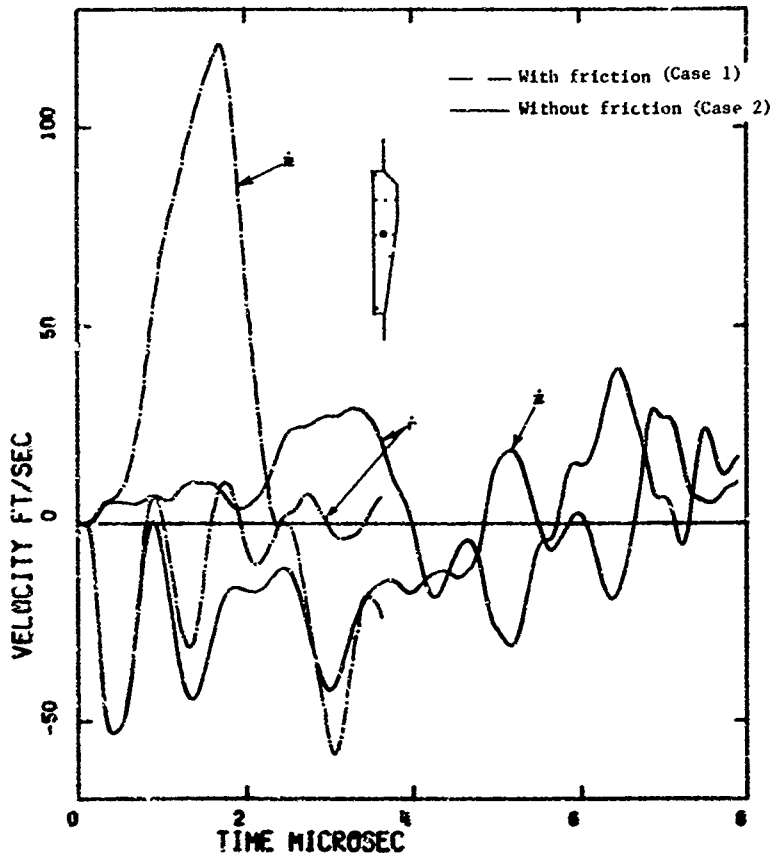


Figure B-5. Velocity Components at Station 5 - Baseline Design

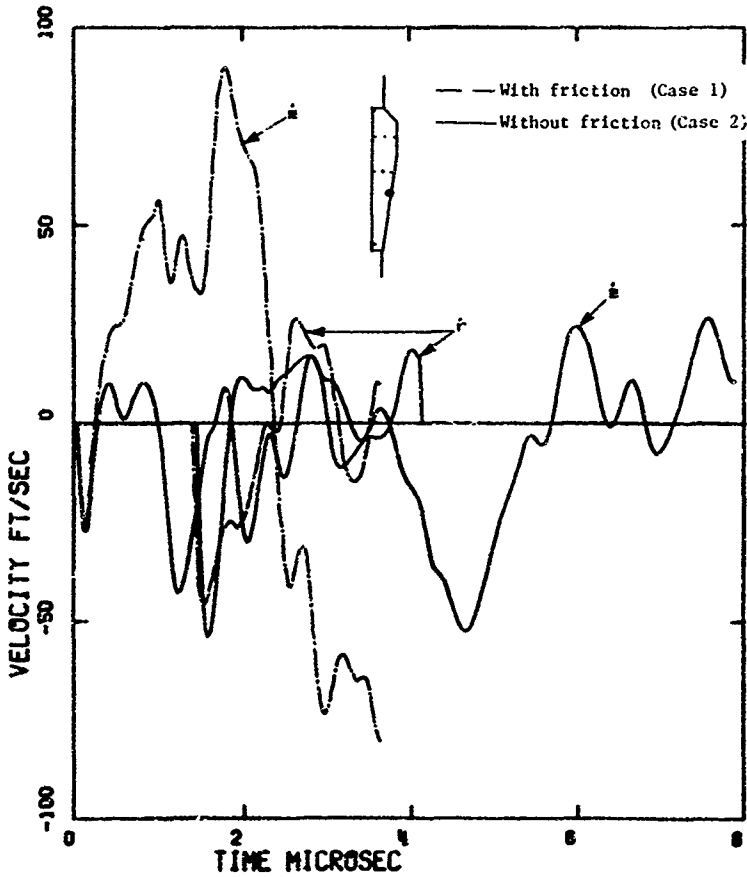


Figure B-6. Velocity Components at Station 7 - Baseline Design

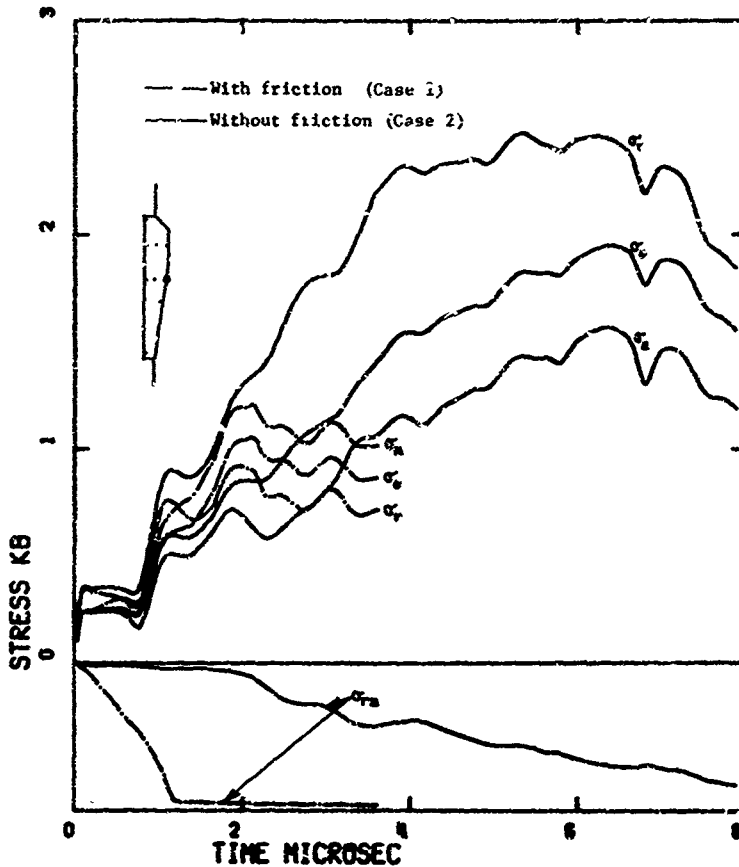


Figure B-7. Stress Components at Station 8 - Baseline Design

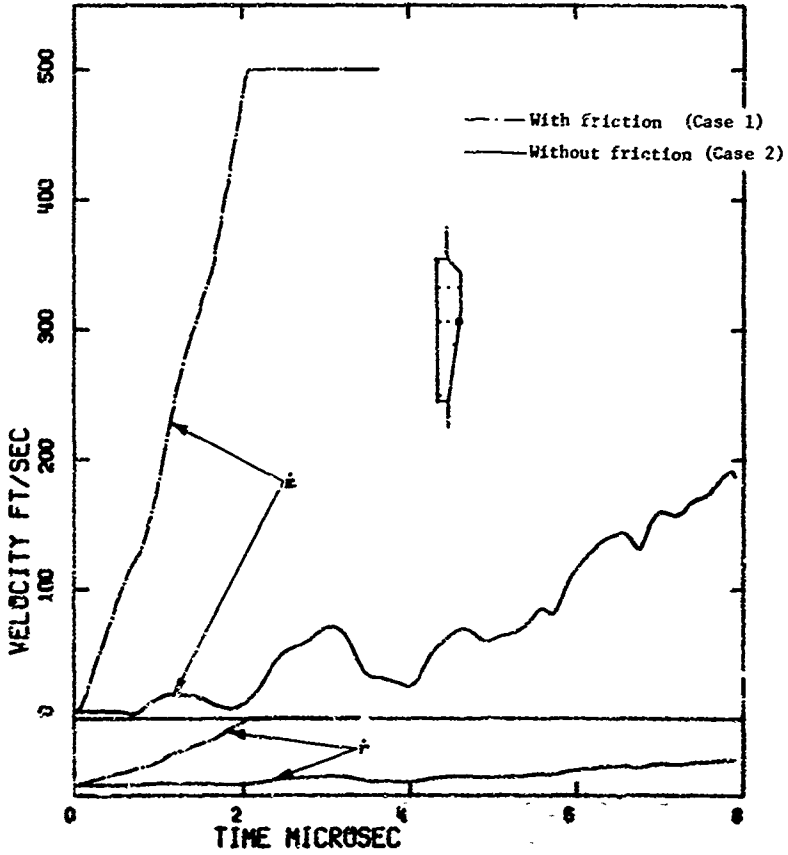


Figure B-8. Velocity Components at Station 8 - Baseline Design

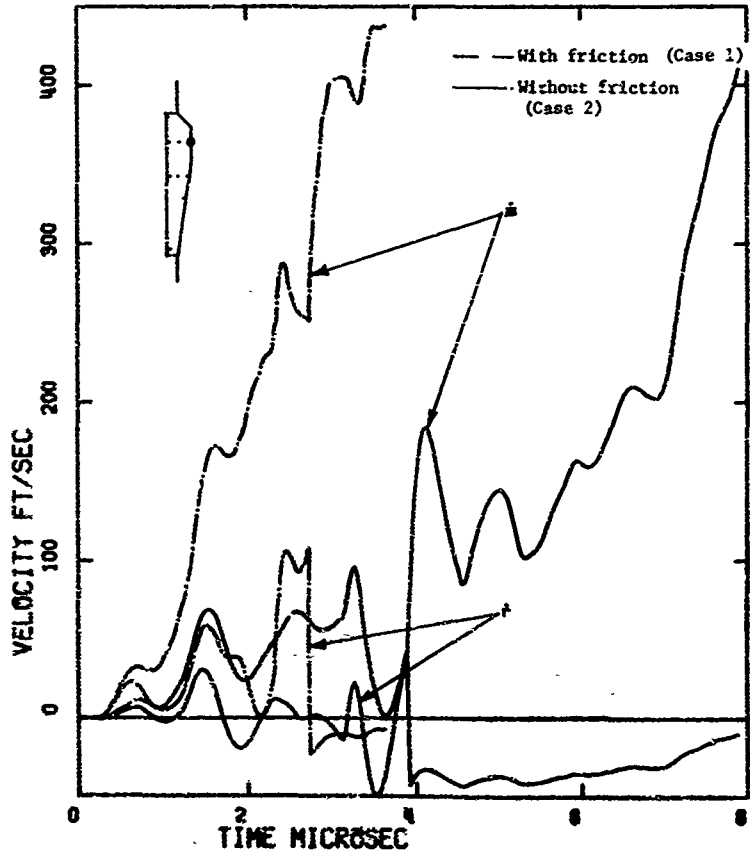


Figure B-5. Velocity Components at Station 9 - Baseline Design

CALIFORNIA RESEARCH AND TECHNOLOGY, INC.
 R&T NO. 2010-G. PLASTIC BAND/CONE INTERACTION
 STATION 2

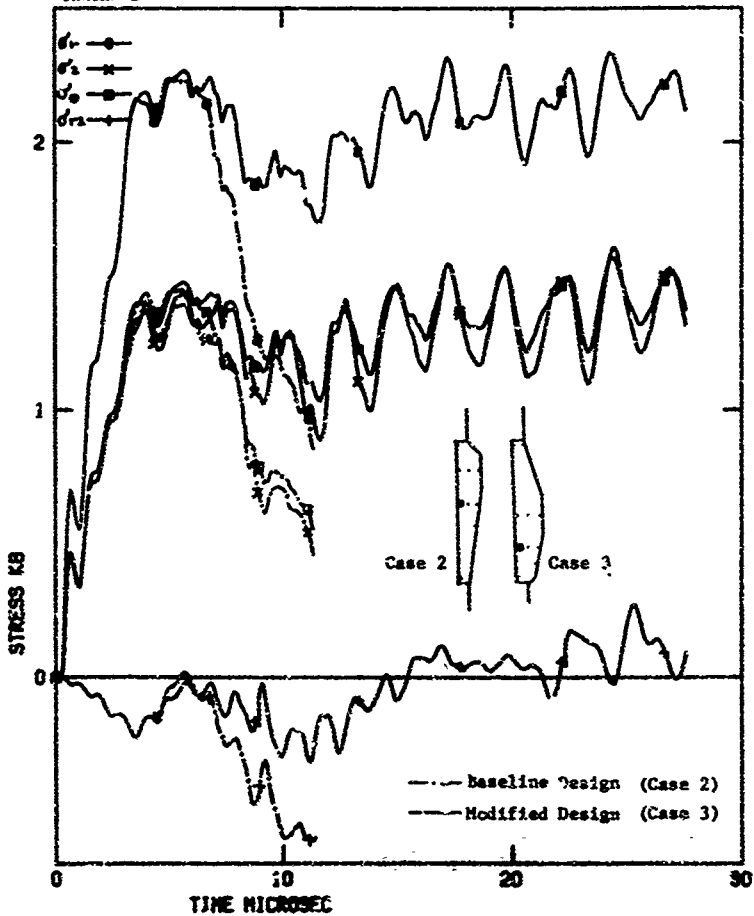


Figure B-10. Stress Components at Station 2, Baseline and Modified Plastic Band Designs

CALIFORNIA RESEARCH AND TECHNOLOGY, INC.
 SAN JOSE, CALIF. PLASTIC BOND/PINE INTERFACIAL
 STATION 3

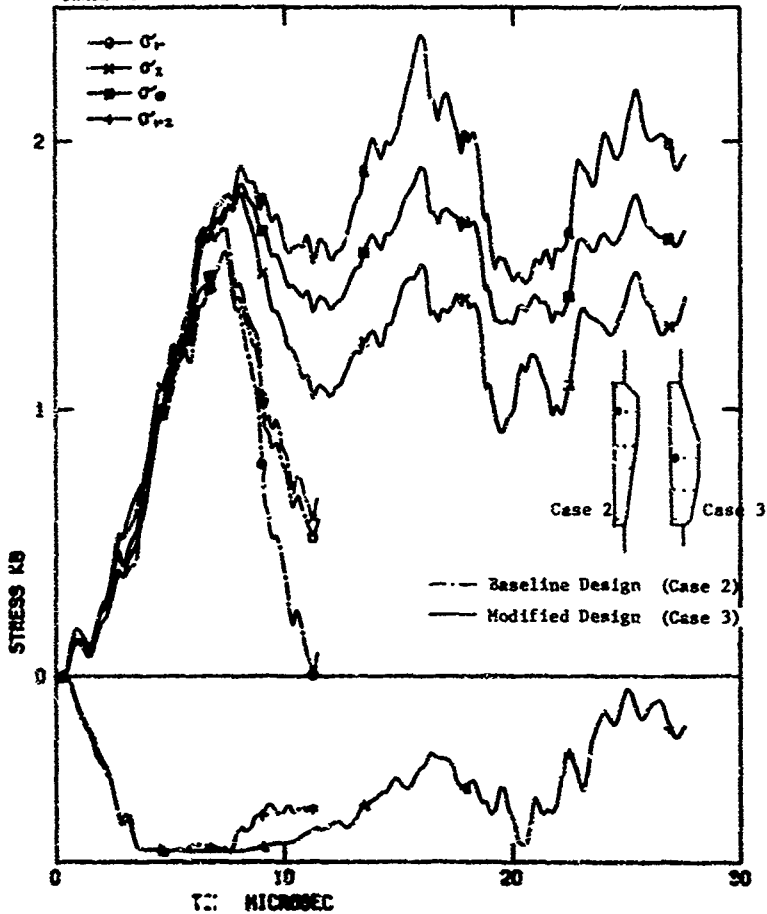


Figure B-11. Stress Components at Station 3, Baseline and Modified Plastic Bond Designs

CALIFORNIA RESEARCH AND TECHNOLOGY, INC.
 RMN NO. 3010-8. PLASTIC BAND/CORE INTERACTION
 SYSTEM 8

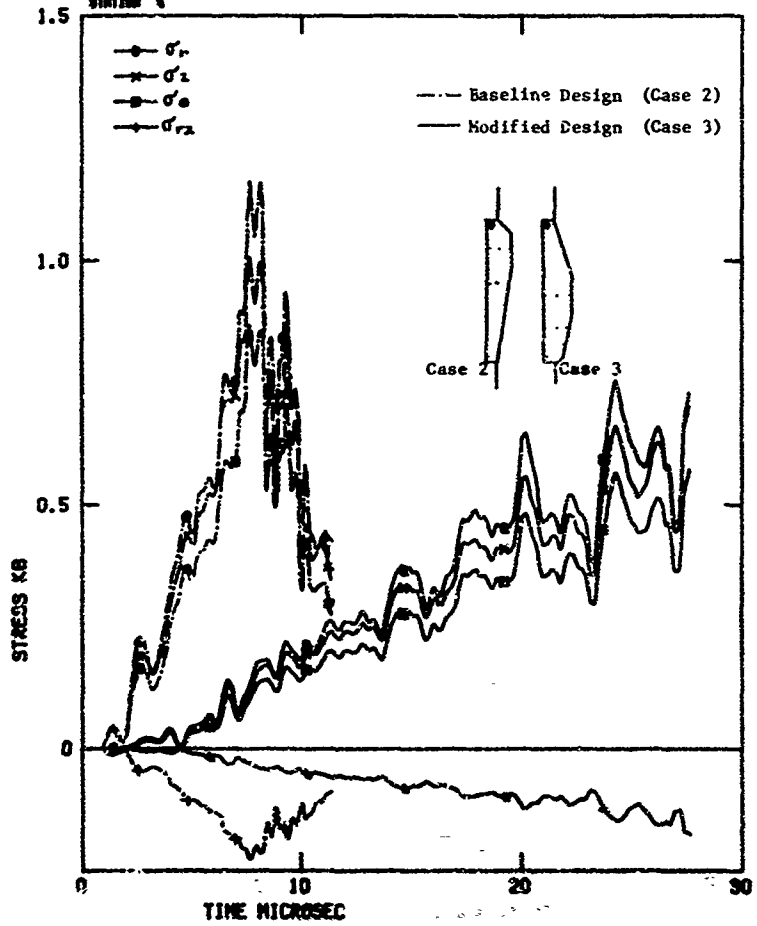


Figure B-12. Stress Components at Station 4, Baseline and Modified Plastic Band Designs

CALIFORNIA RESEARCH AND TECHNOLOGY, INC.
 FOR THE U.S. AIR FORCE PLASTIC AND/ORE INDUSTRIES
 DIVISION 8

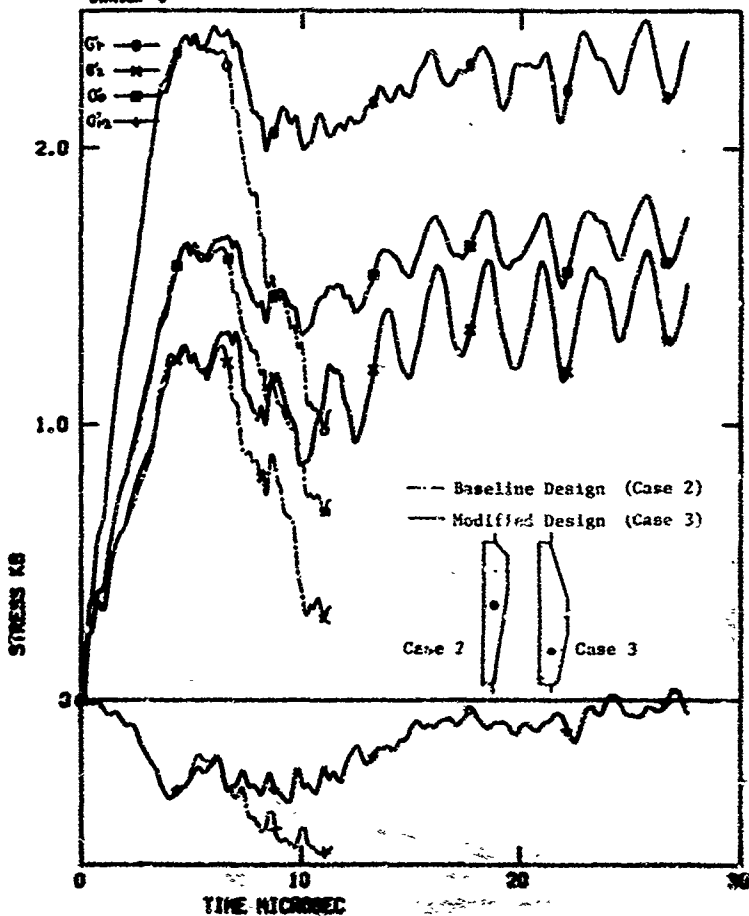


Figure B-13. Stress Components at Station 5, Baseline and Modified Plastic Band Designs

CALIFORNIA RESEARCH AND TECHNOLOGY, INC.
 RM 88, 3640-G, PLASTIC DYNAMIC INTERACTION
 STATION 6

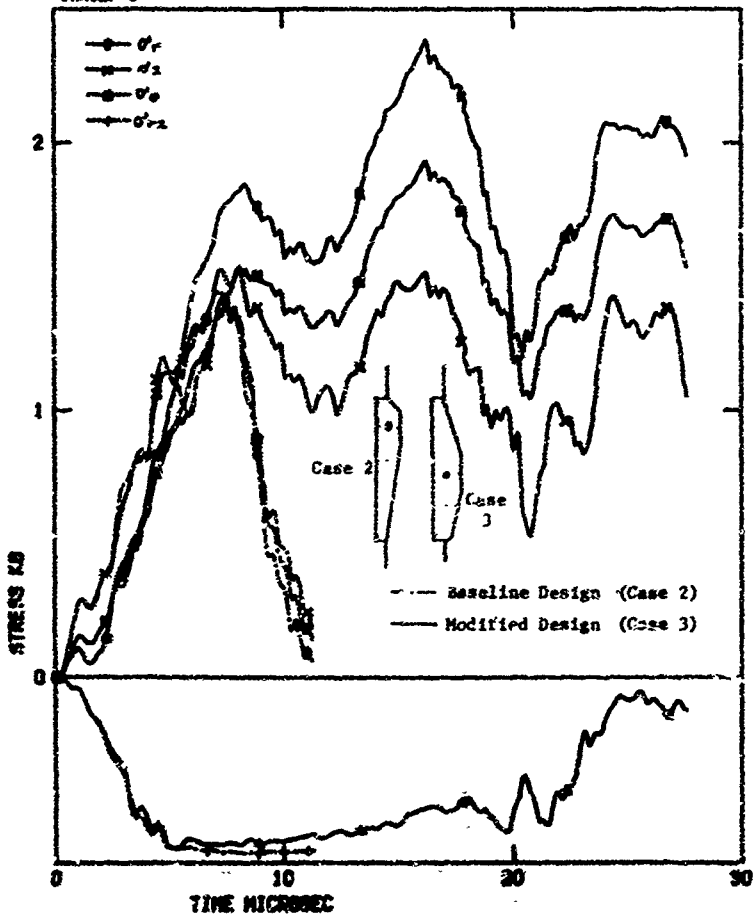


Figure B-24. Stress Components at Station 6, Baseline and Modified Plastic Band Designs

CALIFORNIA RESEARCH AND TECHNOLOGY, INC.
 SD-66-1. PLASTIC SAND/STONE INTERACTION
 STATION 6

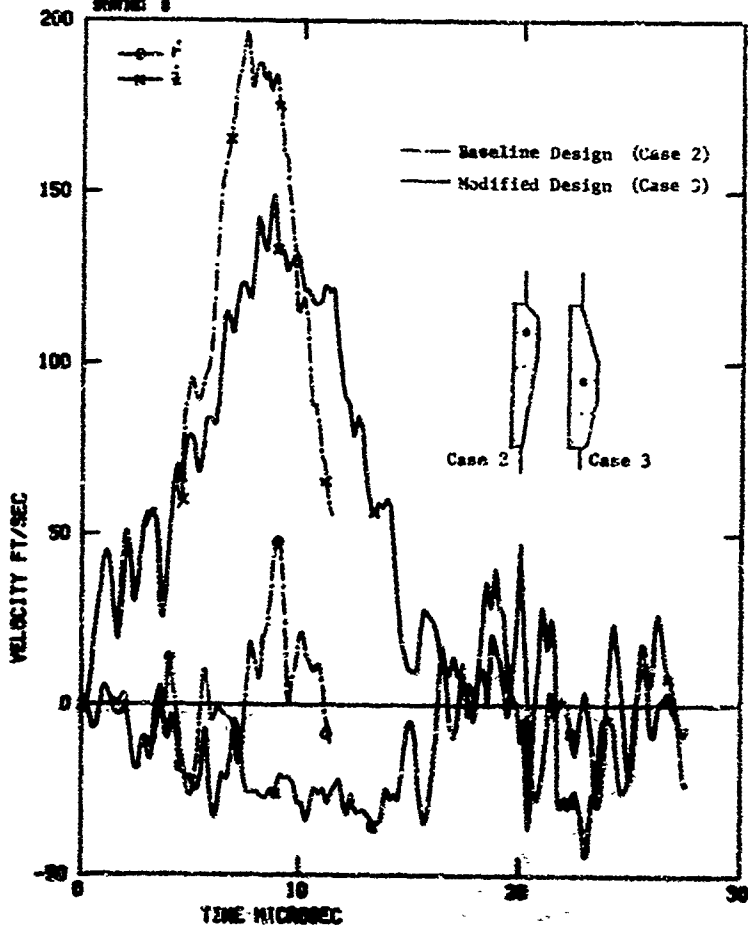


Figure B-15. Velocity Components at Station 6, Baseline and Modified Plastic Sand Designs

OLDFORD RESEARCH AND DEVELOPMENT, INC.
 800 N. 300-E. PLAZA SUITE 200
 JORDAN 6

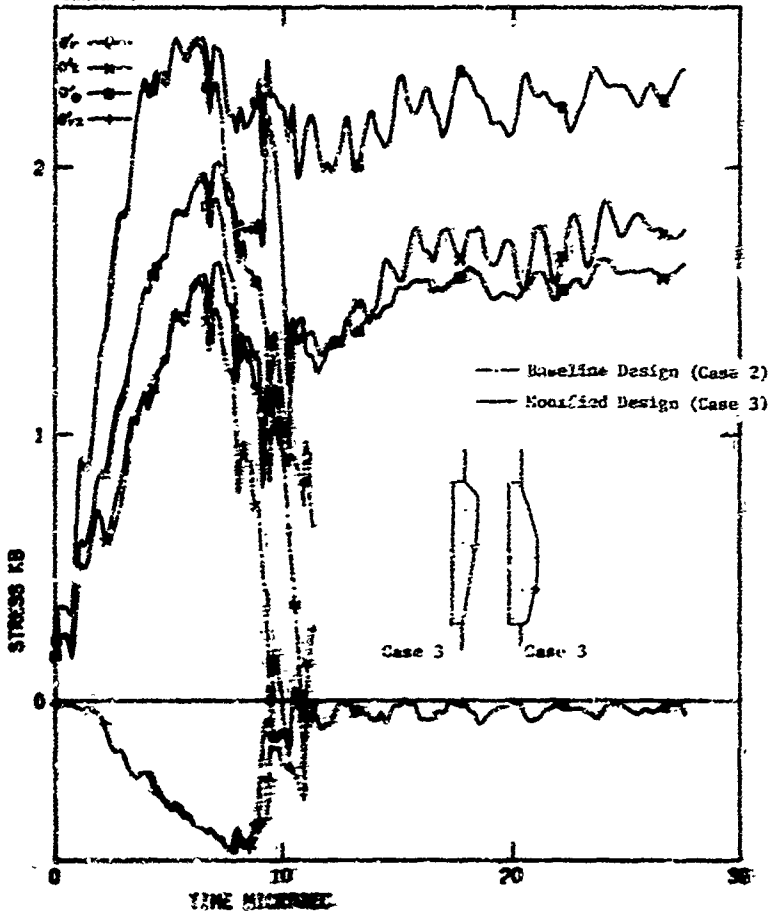


Figure E-16. Stress Components at Station E, Baseline and Modified Plastic Bend Designs

CALIFORNIA RESEARCH AND TECHNOLOGY, INC.
 DR. NO. 300-C, PLASTIC BAND/CRACK INTERACTION
 STATION 0

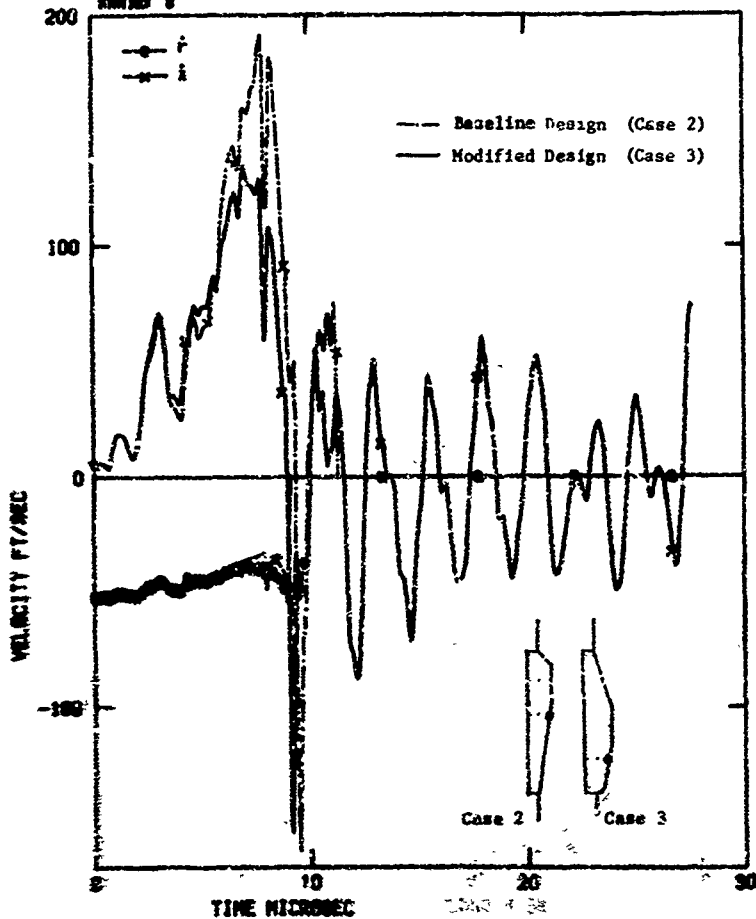


Figure E-17. Velocity Components at Station 0, Baseline and Modified Plastic Band Designs

CALIFORNIA RESEARCH AND TECHNOLOGY, INC.
 RPT. NO. CR-66-4. PLASTIC BOND/CORE INTERACTION
 STATION 9

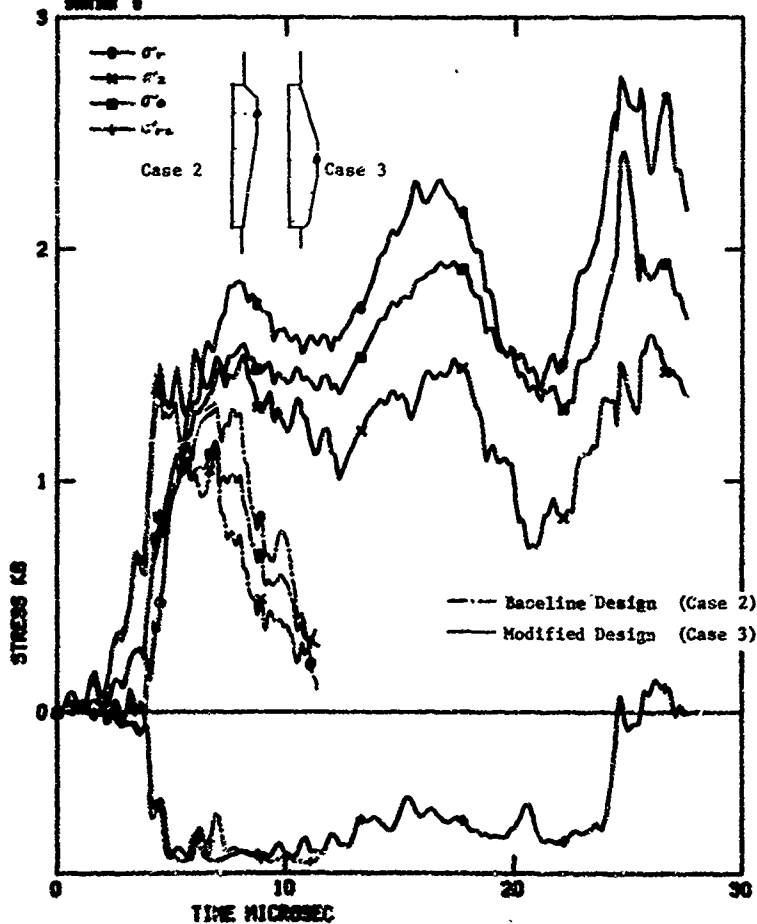


Figure B-18. Stress Components at Station 9, Baseline and Modified Plastic Band Designs

CALIFORNIA RESEARCH AND TECHNOLOGY, INC.
 ITEM NO. 2040-S. PLASTIC BOND/CORE INTERACTION
 STATION 9

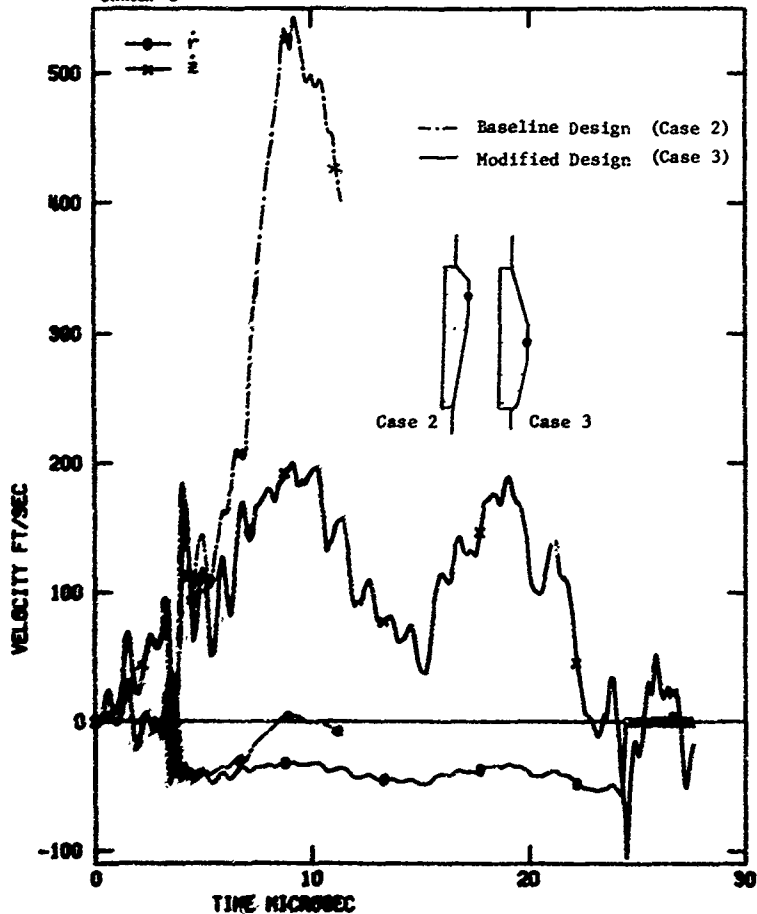


Figure B-19. Velocity Components at Station 9, Baseline and Modified Plastic Bend Designs

REFERENCES

1. M. L. Wilkins, Calculation of Elastic-Plastic Flow, UCRI-7322, Rev. 1, Lawrence Radiation Laboratory, Livermore, CA, January 1969
2. K. N. Kreyenhagen, M. H. Wagner, and W. S. Goerke Direct Impact Effects in Hypersonic Erosion, SAMSO-TR-73-339, Space & Missile Systems Organization, Los Angeles, CA August 1973
3. K. N. Kreyenhagen, M. Rosenblatt, and T. R. Isbelle (California Research & Technology) Cratering, Mass Loss, and Residual Damage to Hypersonic Particle Impacts on Ablative Materials, AFWL-TR-75-184, Air Force Weapons Laboratory, Kirtland AFB, NM, June 1975
4. M. H. Wagner, K. N. Kreyenhagen, and W. W. Goerke (California Research & Technology), Numerical Analysis of DNA Earth Penetrator Experiment at DRES, DNA 3537F, Defense Nuclear Agency, Washington, D.C., October 1974
5. M. H. Wagner, K. N. Kreyenhagen, and W. S. Goerke (California Research & Technology), Numerical Analysis of Projectile Impact and Deep Penetration into Earth Media, WES S-75-4, Waterways Experiment Station, Vicksburg, Miss., August 1975
6. Y. M. Ito, K. N. Kreyenhagen, G. E. Eggum, and W. S. Goerke, (California Research & Technology), Analysis of Dynamic Stresses within a Terminal Delivery Vehicle During Penetration of a Hard Earth Target, WES S-75-1, Waterways Experiment Station, Vicksburg, Miss., February 1975
7. S. W. Tsai, Air Force Materials Laboratory (Personal Communication)